CRYSTAL GROWTH AND PLASTICITY OF VANADIUM DISILICIDE

by

Robert Boyd B.Sc.

Submitted for the degree of Doctor of Philosophy to the University of Warwick.

This research was carried out in the Department of Physics, University of Warwick.

December, 1975

C O N T E N T S

LIST OF FIGURES

LIST OF TABLES

ACKNOWLEDGEMENTS

I would like to thank Professor A. J. Forty for making available to me the facilities of the Department of Physics at the University of Warwick. I should like to thank Dr. M. H. Lewis for introducing me to the fields of ceramic materials and electron microscopy, and for his advice throughout this work and the preparation of this thesis.
I should like to thank Dr. P. S. Bell for many useful discussions and in particular for the use of his computer programmes to generate the stereographic projections reproduced in this thesis. I should also like to thank Mr. G. Smith for his assistance with the preparation of photographs for this thesis and Mrs. D. Jackson for typing the manuscript.
My thanks are due to the Science Research Council and to J. Lucas Ltd. for the provision of a CAPS Research Studentship.
I would like to thank my wife Irene for her unfailing understanding and encouragement throughout the period of this work.

MEMORANDUM

This dissertation is submitted to the University of Warwick in support of my application for admission to the degree of Doctor of Philosophy. It contains an account of my own work performed at the Department of Physics of the University of Warwick in the period January 1971 to January 1974 under the general supervision of Dr. M. H. Lewis. No part of it has been used previously in a degree thesis submitted to this or any other University. The work described in this thesis is the result of my own independent research except where specifically acknowledged in the text.

December, 1975

Robert Boyd

ABSTRACT

Vanadium disilicide (VSi_2) has been studied as a model with a view to evaluating disilicides as high temperature structural materials. The homogeneity range and phase boundaries of VSi_{2-x} have been determined, Evidence has been obtained for the existence of a "new" phase in the V-Si binary system, and a new V-Si phase diagram, including this information, is presented.

Large high-purity single crystals with compositions across the homogeneity range of VSi_{2-x} have been grown by Czochralski pulling from a melt contained in a cold hearth r.f. levitation crucible. A compression testing programme was carried out on these crystals in the temperature range 600-1200^{o}C. Analysis of the compressed crystals by optical metallography and transmission electron microscopy showed that in the temperature range studied VSi_2 deformed by basal slip only. Defect structure consisted typically of paired dislocations which were shown to be mainly dislocation dipoles. A model for plasticity in VSi_2 has been proposed. Slip is initiated by overcoming of a Peierls barrier. There is a two-stage work-hardening curve. Stage I (high) hardening is due to dipole formation. Stage II is a region in which a dynamic recovery process occurs by dislocation climb and annihilation of loops formed from dipoles. Experimental evidence from temperature, composition and strain rate dependence has been used to justify this model.

The lack of slip flexibility in VSi_2 emphasises that it will be difficult to prepare an engineering material to fully utilise the good strength retention and oxidation resistance at high temperatures found in disilicides. However, the use of disilicides either in the form of very fine-grained polycrystalline material or as the fibrous phase (with the c-axis as the fibre axis) in a ductile (metallic) matrix has been suggested as the most promising potential use for transition metal disilicides as structural materials.

CHAPTER 1

INTRODUCTION

1.1 High Temperature Materials

Modern technology has an increasing requirement for engineering materials which have high strengths and large elastic moduli but have low density. For many applications these materials must exhibit good stability and strength retention at working temperatures in excess of 1000°C. The search for new materials to meet these stringent requirements has been concentrated in the last decade on what have been named "inherently strong solids"[1]. Some characteristic features expected to be shown by the crystal structure and chemical composition of these strong solids may be deduced by considering the theoretical strength of a solid.

The theoretical fracture stress σ_{max} for any solid is given by [2]

$$\sigma_{max} = \sqrt{\frac{E\gamma}{a_o}} \qquad 1.1$$

where E is Young's modulus for the appropriate direction in the solid, a_o is the equilibrium separation of atomic planes and γ is the surface energy.

Equation 1.1 implies that a high breaking strength requires a high Young's modulus, large surface energy and small separation of atoms. Crystals with covalent and metallic bonding have the highest values of σ_{max} since in ionic solids electrically neutral planes can be cleavage planes of low surface energy. Of the metals the transition metals have the highest values of σ_{max} .

The theoretical shear strength, τ_{max}, is given by [3]

$$\tau_{max} = \frac{Gb}{2\pi h} \qquad 1.2$$

where G is the shear modulus, b the interatomic distance in the direction of shear, and h the interatomic distance perpendicular to b in the plane of shear.

To ensure a high theoretical strength, both the shear modulus G and the value of τ_{max}/G should be as large as possible. This indicates a solid in which the interatomic forces are strongly directional, as in solids with covalent or strongly polarised ionic bonding. For a large value of elastic modulus in a covalent solid, small atoms and short bond lengths are required so that a high density of directional bonds is produced. Similarly, in an ionic solid, small ions of high charge are required.

An ideally strong solid will possess large values of both τ_{max} and σ_{max}. Metals have low values of τ_{max}/G because of their lack of directional bonding, and have shear strengths controlled by mobile dislocations which move at stresses much smaller than the theoretical value τ_{max}. In spite of this, metals have only recently been challenged as the principal strong engineering materials, because techniques such as solution hardening and dispersion hardening, which inhibit dislocation motion, have been developed to such a degree that the best steels may achieve strengths up to 250 kg/mm^2 at room temperature. The limit of development of these steels has been reached, and to improve markedly on the strengths achieved, particularly at high temperatures (where

even the best steels show poor oxidation resistance and strength retention) inherently strong solids with a high τ_{max}/σ_{max} ratio must be used.

Materials which satisfy this requirement are beryllium boron, carbon and compounds containing either these elements or one of the elements N, O or Si as one (or more) component, e.g. WC, BN, Si_3N_4, Al_2O_3. Some additional advantages derive from this τ_{max}/σ_{max} criterion. The requirement for small atoms ensures that the lighter elements are present, and the directional bonding implies non-close-packed crystal structures. The density of an inherently strong solid will therefore be expected to be low. A large elastic modulus implies a high binding energy, hence a good stability and a high melting point are expected. This combination is ideal for high temperature applications.

Strong crystalline solids which have a large value of τ_{max}/G have an inherent resistance to dislocation motion and their strength at low temperature is normally dependent on the presence of surface steps or cracks which initiate brittle fracture. Inherently strong crystals frequently have structures with non-cubic symmetry which makes it unlikely that a multiplicity of slip systems will be operative when dislocation motion does occur, at higher temperatures. Hence, it is unlikely that the von Mises crition of five independent slip systems [4] for deformability of poly-crystalline material will be satisfied.

To achieve experimentally the high theoretical strengths of inherently strong solids is therefore very difficult. The two main lines of approach have been (i) the production of

ultra-fine grained polycrystals, thereby reducing the possibility of larger Griffith cracks, and (ii) the use of strong solids in composite materials, e.g. fibres in a metallic matrix. Single crystal whiskers of graphite, sapphire, Si_3N_4 SiC and AlN are the materials whose strengths (1-3 x 10^3 kg/mm^2) experimentally approach the theoretical most closely.

1.2 Transition Metal Silicides

This thesis is concerned with the assessment of transition metal disilicides ($MeSi_2$) as potential high temperature materials using vanadium dislicide VSi_2 as a model compound.

1.2.1 The Hybrid Nature of Silicides

Silicides occupy an intermediate position between interstitial and intermetallic compounds in terms of crystal structure and bonding characteristics.

Hägg[5] has defined interstitial compounds by putting an upper limit on the non-metal to metal atomic radius ratio r_x/r_m, i.e. defining the size of an interstitial site in a metal in terms of the metal atom radius, and setting this as the upper limit or the size of the potential interstitial non-metal atom. He gave as the limiting condition

$$r_x/r_m \leq 0.59 \qquad 1.3$$

which is equivalent to allowing H, B, C and N atoms only as possible interstitials. This definition excludes Si as an interstitial, although many silicides can be regarded as true interstitial compounds.

A more meaningful definition of an interstitial compound must consider the nature of the bonding in that compound as

well as geometrical limits. An interstitial compound may be defined as one in which the metal-metal atom (Me-Me) bond remains the dominant type, the non-metal atoms being sufficiently small to be accommodated within the metal-atom substructure with a limited degree of distortion of the metal structure. This more flexible definition admits as interstitial compounds the lower silicides of the transition metals of groups IV and V, e.g. Hf_2Si and Nb_4Si. With increasing silicon content, a progressive increase in covalent Si-Si bonding similar to that of B-B bonds in the transition metal borides is observed[6]. This may be summarised as follows. In a typical transition metal-silicon system the bonding develops with increasing silicon thus:

(i) Isolated Si atoms bonded to metal atoms only (V_3Si, Cr_3Si);

(ii) Isolated pairs of Si atoms (U_3Si_2);

(iii) One-dimensional chains of Si atoms (Me_5Si_3 types);

(iv) Two or three dimensional frameworks of Si atoms ($MeSi_2$ types)

This increase in Si-Si covalent bonding progressively destroys the interstitial nature of the higher silicides. In the highest silicides, $MeSi_2$, the Si atoms occupy substitutional sites also. Estimates of bonding character in disilicides using data on heats of formation[7] have confirmed the increasing concentration of strong Me-Si bonding at the expense of Me-Me bonding. Although the covalent Si-Si bonding is also increased, the nature of the Me-Si bond along with the residual Me-Me bonding explains the metallic properties of most disilicides (e.g. good electric and thermal

conductivity). This effectively means that when bonded in higher silicides the Si atom may be regarded as a metal, and these disilicides can justifiably be regarded as inter-metallic compounds ordered up to their melting points.

1.2.2 Transition Metal Silicides as Structural Materials

Transition metal silicides are inherently strong solids as described in section 1.1. The occurrence of silicide compounds in transition metal-silicon binary systems is summarised in Fig. 1.1.

The increase in density of directed bonds with increasing Si content implies that the higher silicides, particularly $MeSi_2$ have the highest value of theoretical strength of the silicides, and these values should be comparable with, for example, the transition metal mono-carbides MeC which are true interstitial compounds and are themselves of current interest as high temperature materials.

The intermediate Me_5Si_3 and higher $MeSi_2$ silicides have melting points in the range 1500 to 2000°C which compares unfavourably with typical values of 3000°C for the transition metal mon-carbides. The disadvantage of lower melting point of the silicides may well be outweighed by consideration of the chemical stability of the silicides.

The disilicides have been shown to exhibit excellent oxidation resistance[8] up to 1200°C and good corrosion resistance properties which are markedly superior to those of alloy steels and transition metal carbides.

Silicides exhibit excellent thermal shock resistance. Data on thermal conductivity[9] shows silicides to have superior properties to most other inherently strong solids.

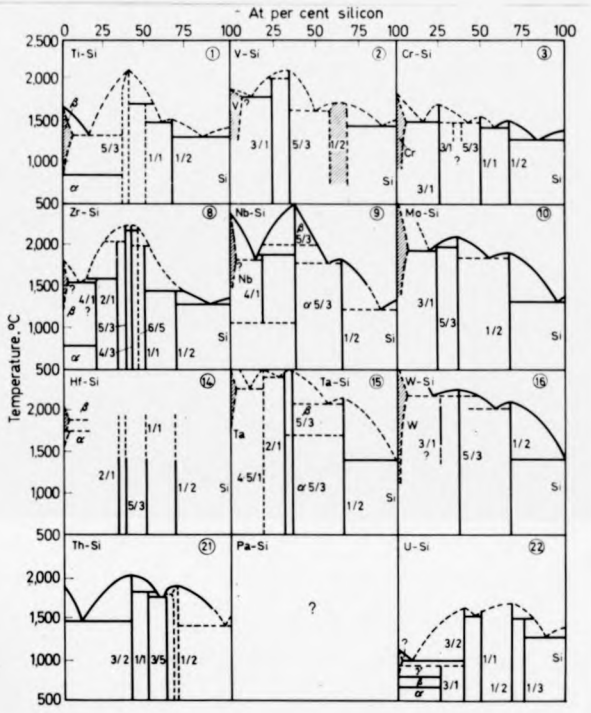

Fig. 1.1 Me-Si binary phase diagrams (after Goldschmidt[6])

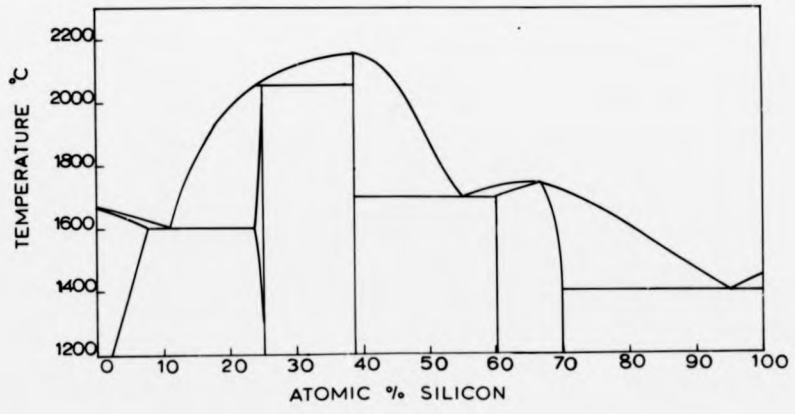

Fig. 1.2 V-Si phase diagram (after Efimov[10])

Ease of preparation is an important point to be considered in any material selection programme. Transition metal silicides, particularly the higher silicides are almost all congruently melting compounds which facilitates their preparation as single phase homogeneous material by conventional metallurgical techniques.

The higher silicides Me_5Si_3 and $MeSi_2$ are in most cases "layer" structures, i.e. they consist of stacking sequences of metal and/or silicon layers in a particular configuration. As such their crystal structures and hence their properties tend to be markedly anisotropic. These materials therefore are not likely to satisfy the von Mises criterion[4] for slip flexibility. Glide within the stacked layers is the most likely primary slip system, as in h.c.p. metals. The bonding connecting layers is largely Si-Si bonding. Slip out of the relatively close-packed layer is unlikely - the Burgers vector will be large and hence energetically unfavourable. A limited number of independent slip systems is anticipated. This is in direct contrast to the transition metal mono-carbides which generally have cubic symmetry because of their interstitial nature, and have a multiplicity of independent slip systems.

Because of their lack of slip flexibility, it is important that silicides may be prepared in the form of fine-grained polycrystals to restrict crack length and maximise grain-boundary diffusion mechanisms - both of which improve plasticity of polycrystalline material. Here again congruent melting of disilicides means that rapid solidification techniques will produce fine-grained single-phase material.

There is every indication that transition metal silicides are promising high-temperature structural materials.

1.3 The Vanadium-Silicon System

The V-Si system was selected as being typical of the binary transition metal-silicon systems of Fig. 1.1. The melting points of the vanadium silicides are lower than average, thus facilitating materials preparation, crystal growth and mechanical testing.

1.3.1 Phase Equilibria and Crystal Structure

The V-Si phase diagram, Fig. 1.2, is that due to Efimov[10]. The main features of this diagram have been confirmed by other workers[11]. A comparison of Figs. 1.1 and 1.2 shows that the V-Si system is typical of the binary systems, containing several congruently melting silicides with relatively high melting points and high eutectic temperatures. The main contrast between this and a typical transition metal-carbon diagram is the small difference in melting points of the various silicides and between melting and eutectic temperatures.

V_3Si, the lowest silicide, has space group O_h^3 and cell parameter a = 4.722Å. This structure is known as β-W (W_3O) and is shown in Fig. 1.3. It can be regarded as being derived from the b.c.c. parent metal, and is therefore an interstitial compound in which the metallic V-V bond is predominant. V_3Si is isomorphous with Cr_3Si, Mo_3Si and probably W_3Si, and U_3Si is a tetragonal variant of the β-W structure. These silicides have attracted great attention because of their superconducting properties. V_3Si in particular has one of the highest superconducting transition temperatures known, 17.5°K.

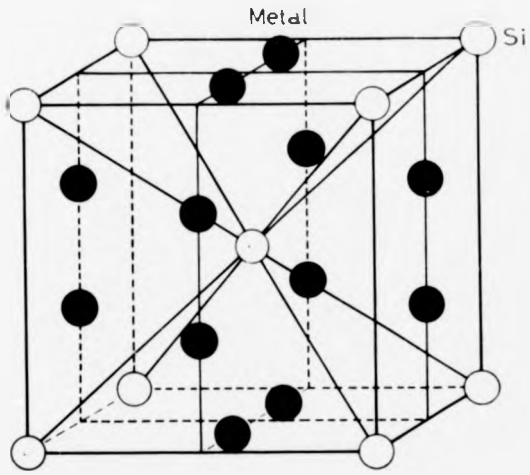

Fig. 1.3 V_3Si crystal structure

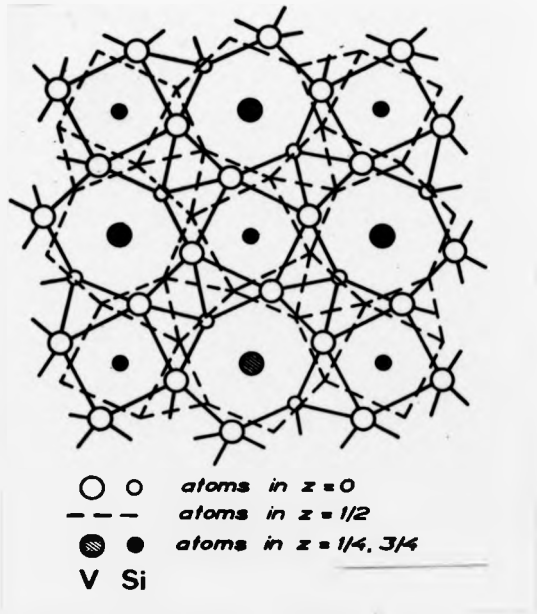

Fig. 1.4 V_5Si_3 layer structure

V_5Si_3 is the intermediate silicide and has the highest melting point in the V-Si system -2150°C. This phase has tetragonal symmetry, space group D_{4h}^{18}, unit cell dimensions a = 9.429Å; c = 4.757Å, and consists of metal atom layers which take up Si atoms both substitutionally and interstitially, as shown in Fig. 1.4. The Si atoms are linked in one-dimensional chains, i.e. the Si-Si bond is present, but does not entirely destroy the interstitial nature of the phase. All the Me_5Si_3 and Me_3Si_2 phases are isomorphous or closely related. V_5Si_3 is isomorphous with the intermediate silicides of W, Nb, Ta, Cr and Mo, designated the W_5Si_3.type. These intermediate phases have been extensively studied by Nowotny[12]. He has shown that the silicides with the closely related Mn_5Si_3 structure, in which all Si atoms are on metal sites, are in most cases ternary phases which contain small amounts of C, B or N which occupy interstitial sites, displacing Si atoms entirely on to substitutional sites, thus "stabilising" the higher symmetry Mn_5Si_3 structure. Such compounds are known as "Nowotny phases" and include Ti_5Si_3, Mo_5Si_3 (C), Cr_5Si_3 (C, B or N).

The highest silicide formed is the disilicide VSi_2, which has the most promise as a refractory material. This is the compound studied in this research. VSi_2 has hexagonal symmetry, space group D_{6h}^4 lattice parameters a = 4.571Å, c = 6.372Å. The structure consists of a three-fold repeat stacking sequence of close-packed layers as shown in Fig. 1.5. Figure 1.6 shows in more detail a (0001) projection of the three-layer repeat stacking sequence. VSi_2 is isomorphous with $NbSi_2$, $TaSi_2$ and $CrSi_2$. There are two other closely

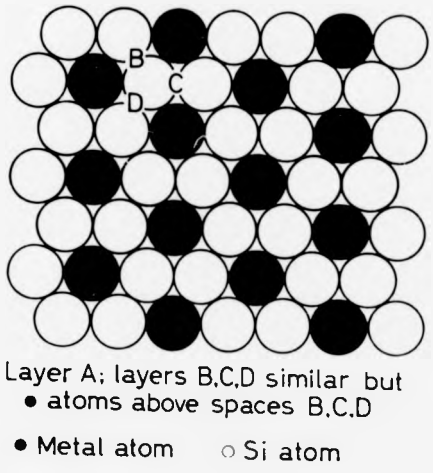

Fig. 1.5 VSi_2 layer structure

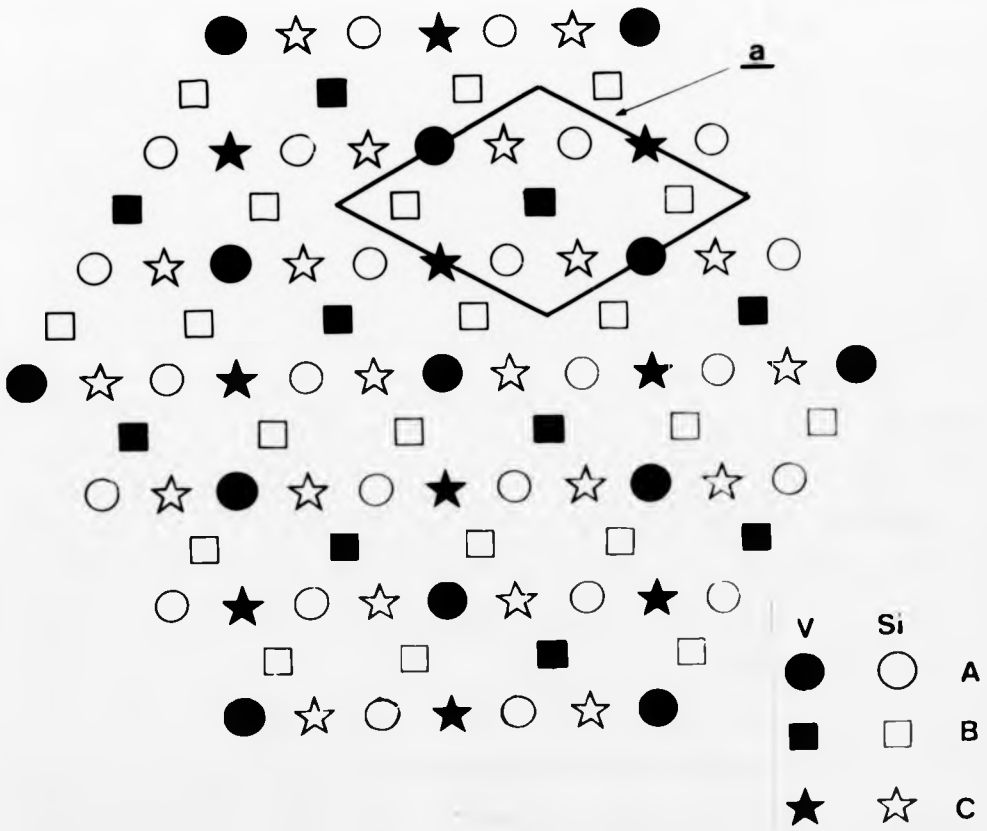

Fig. 1.6 VSi_2 (0001) projection

related groups of disilicides - the $MoSi_2$ and $TiSi_2$. These are respectively two- and four-fold repeat stacking sequences of similar close-packed Me-Si layers. It is important to note that the stacking of layers in VSi_2 does not give a close-packed structure. The layer displacements are such that V atoms lie not above octahedral holes as in h.c.p. metal stacking, but above saddle-points. The three-fold stacking sequence with the V atoms stacked in saddle positions gives the six-fold symmetric screw-axis, which gives the hexagonal symmetry of the structure. There are two important consequences of this structure. The first is the possibility of enantiomorphic forms of VSi_2, i.e. a reversal of the stacking sequence from ABCABCA to ACBACBA. Secondly, the possibility of stacking faults must be considered. Both of these aspects will be considered in more detail below. The findings of Robins and Jenkins[7] confirm the predominance of the strong V-Si bond with the covalent Si-Si bond less important. VSi_2 can be regarded as an intermetallic compound which does contain some directional bonding. The phase diagram, Fig. 1.2, indicates that VSi_2 has a large homogeneity range. Phase boundaries are not precisely known for VSi_2 or other disilicides, although some evidence for a homogeneity range for $CrSi_2$ of $CrSi_{1.9}$–$CrSi_{2.6}$ has been found[13], and in the closely related diborides deviations from stoichiometry are very common. In view of the pronounced influence of non-stoichiometry on mechanical deformation and other properties, the extent and possible mechanisms for accommodation of non-stoichiometry have been studied in the present research on

VSi_2. As a prelude to this study a general review of the various mechanisms for the structural accommodation of non-stoichiometry will be given in the following section.

The close analogy between the silicides of vanadium and those of the other transition metals shows that the V-Si system is a good model for transition metal-silicon binary systems, and that the work described in this thesis for VSi_2 may be used in predicting the qualitative behaviour of other structurally similar disilicides.

1.3.2 Structural Accommodation of Non-Stoichiometry

The early work of Hägg[5] and Kurnakov[14] on interstitial and intermetallic compounds respectively demonstrated the occurrence of compounds which retained the same crystal structure over a range of compositions. This was contrary to the Law of Definite Proportions which stated that in any compound the elements should be present only in simple integral ratios. This remained a topic of controversy until the work of Schottkey and Wagner[15] based on statistical mechanics, showed that the occurrence of a compound at a simple integral atomic ratio, i.e. a "stoichiometric" composition is the limiting case, and that all inorganic crystalline compounds should be considered as having a composition range. It is usual to draw a distinction between compounds whose composition range is small, less than 0.1% atomic, in which the deviation from stoichiometry can be regarded as a statistical fluctuation, and those with gross deviations from stoichiometry in which interactions between non-stoichiometric defects are important. The latter are

classed as non-stoichiometric compounds. The approximate experimental data available for VSi_2 (Fig. 1.2) indicates that it may accommodate large departures from the stoichiometric VSi_2 composition.

A general classification of possible mechanisms for accommodation of gross non-stoichiometry has been given by Wadsley[16].

For a compound of elements M and X, the possible modes of accommodating non-stoichiometry may be subdivided.

(a) Substitution of one element M or the sublattice of the other, X. This is a common mechanism in intermetallic compounds.

(b) Interpolation. An excess of M or X can be accommodated in interstices in the structure. This mechanism is restricted to compounds containing large interstices or relatively small atoms of one component, and is not the most probable mechanism in VSi_2.

(c) Subtraction. Either M or X (or both simultaneously in unequal concentrations) may be absent from the structure. This mechanism is common in transition metal oxides and carbides. The non-stoichiometric vacancies in some of these compounds adopt ordered configurations at low temperatures.

(d) Shear Structures. This is a special case of subtraction in which the vacant sites are ordered in a planar form. Such planes constitute boundaries between blocks of unchanged structure and are known as shear planes. In the simplest cases the shear planes are parallel and regularly spaced. These have been observed mainly in oxide systems, and homologous series of structures with general formulae such as

TiO_{2n-1} for m = 4,5 . . . 10 have been identified[17]. Recent work[18] has identified shear structures in the Mn-Si system associated with Mn_5Si_3.

(e) Intergrowth. The parallel microscopic intergrowth of two phases of different composition can occur. The structures of the two phases are usually closely related. This mode has been observed in mixed oxide systems.

The most likely mechanism operating in VSi_2 is either substitution or subtraction. A distinction between these two mechanisms should be possible by a comparison of X-ray and pycnometric density for compounds with extreme deviations from stoichiometry. A lattice parameter variation with composition may also be detectable. An attempt to identify the nature of non-stoichiometric defects in $VSi_{2 \pm x}$ is described in Chapter 3.

The effect of non-stoichiometry on mechanical properties is of particular relevance to the research described in this thesis, and this will be discussed in the following section on mechanical properties.

1.4 Mechanical Deformation of Strong Solids

In view of the hybrid nature of silicides, a brief review of the mechanical properties of intermetallic and interstitial compounds will be given in this section.

1.4.1 Intermetallic Compounds

A comprehensive review of the early literature on mechanical properties of intermetallic compounds has been given by Westbrook[19] and of later work by Lawley[20] and Stoloff[21].

Intermetallic compounds are characterised by high hardness and limited ductility, and after an initial period of routine evaluation of these properties the emphasis has been on explaining them in terms of crystallography and deformation and strengthening mechanisms.

Single crystal deformation studies have been made on the intermetallic compounds AgMg, NiAl, $CuAl_2$ and Mg_3Cd. Most of the work has been done by compression testing because of the brittleness of these compounds at low temperatures and the problems of machining specimens or grip systems suitable for high temperature tensile testing. Conventional two surface trace analysis has been used to determine the slip geometry of intermetallics at elevated temperatures, and it is found that the general features of this geometry are similar to those of metals, i.e. slip occurs in close-packed directions and on planes of highest atomic density. Dislocation motion is the main deformation mechanism, hence strengthening mechanisms are aimed at reducing dislocation mobility. Solid-solution hardening, precipitation hardening, strain hardening and strain ageing are therefore important modes of strengthening as in metals. The deformation mechanisms of intermetallics do differ in some respects from metals. The Burgers vector $\underline{b}$ in intermetallics tends to be large because of the larger unit cells in intermetallic structures. This means that dissociation of perfect dislocations into partials is very important, tending to lead to restriction of slip flexibility and hence to lack of ductility of polycrystalline material. Ductility of poly-

crystals is also restricted by anisotrophy of crystal structure often found in intermetallics. This is particularly relevant in the case of VSi_2. The Peierls stress in intermetallics tends to be large because of directed bonding and large Burgers vector $\underline{b}$. This implies a high flow stress, and limited low temperature ductility. This will be discussed in more detail with specific reference to VSi_2 in a later chapter. Another consequence of a high Peierls stress is that at elevated temperatures diffusion-controlled mechanisms may become rate-determining. Again this will be discussed in more detail later.

Deviations from stoichiometry in intermetallic compounds have a pronounced effect on mechanical properties. Relatively high equilibrium concentrations of point defects are present, usually substitutional defects in the case of intermetallics, at off-stoichiometric compositions. These defects lower the degree of ordering in the compound. VSi_2 is almost certainly ordered up to its melting point. The effect of point-defect disordering on mechanical deformation is a combination of two competing processes. Dislocation interactions with point defects lead to an increase in flow-stress, whereas substitutional and vacancy defects enhance diffusion rates and the deformation mechanisms controlled by them are more easily activated. At low temperatures the net result is a strengthening with deviation from stoichiometry, and at higher temperatures a lowering of strength occurs. This effect has been confirmed in AgMg and Ni_3Al[22].

In addition to the basic research work outlined above, development programmes have been carried out on intermetallics to obtain high-temperature materials. The most promising group so far are the beryllides of transition metals, e.g. $NbBe_{12}$, Nb_2Be_{17}, Nb_2Be_{19}, $TaBe_{12}$. These compounds have been shown to have breaking stresses of the order of 50 kg/mm^2 at 1350^{o}C, but have limited low-temperature ductility. Compounds in the Ti-Ni system have good room temperature strength - 120 kg/mm^2, and have in addition excellent low-temperature ductility, 7-10%.

1.4.2 Interstitial Compounds

Transition metal carbides are the only interstitial compounds which have been extensively studied from the point of view of mechanical properties of the bulk material. Most of the early work was done on sintered compacts of carbides and consisted of determination of Young's moduli, bend strengths and microhardness. The porosity of such samples made the value of these results extremely limited and comparison of results difficult. Only in the last decade with the advent of mechanical testing of fully dense single crystal and polycrystalline material has a meaningful picture of the carbides' mechanical properties emerged.

At room temperature the carbides undergo little if any plastic deformation and brittle fracture occurs at high stress levels. At higher temperatures, usually >0.4Tm, carbides deform plastically by dislocation motion. This behaviour is typical of the difference between interstitial compounds and intermetallics, where macroscopic plasticity often occurs at room temperature. This reflects the

difference in bonding, as well as absolute melting-point. The primary slip system has been shown by single crystal work to be $\{111\}\langle\bar{1}10\rangle$ both for TiC[23] and $VC_{0.84}$[24] and operates at temperatures above 800°C. This is also the primary slip system for f.c.c. metals and both for them and the carbides the Burgers vector $\underline{b}$ is the shortest possible. This close analogy of carbides and metals emphasises that the structure of carbides is closely related to the f.c.c. metal structure which is distorted only slightly by the carbon atom occupation of octahedral interstitial sites in the carbides. The fact that $\{111\}\langle 110\rangle$ is the primary slip system in carbides is very important because it provides five independent slip systems, satisfying the von Mises criterion for macroscopic plasticity of polycrystals. This means that in principle single crystal material is not necessary for engineering applications of carbides. The achievement in practice of this polycrystalline ductility requires the elimination of pores, which act as stress raisers under load and initiate Griffith cracks.

Transition metal carbides fail in a brittle fashion at temperatures below about 800°C because the stress required for dislocation motion at these low temperatures is so high that the competing mechanism of brittle fraction occurs. Dislocation motion in carbides is not fully understood. The low dislocation mobility at low temperatures is usually attributed to a high Peierls stress, and strain-rate dependence of flow stress experiments support this view[23]. At intermediate homologous temperatures below about 0.3 T_m.

self-diffusion of carbon has been suggested as the rate-controlling mechanism of plastic flow, and at higher temperatures, above 0.5 Tmm self-diffusion of the metal is postulated as being rate-determining. However, the activation energies for diffusion in carbides are controversial and inexactly known, and quantitative justification of diffusion-controlled mechanisms has not been possible.

The ductility which can be achieved in polycrystalline carbides which, with their inherent strength, makes carbides very useful in the 800-1100°C temperature range but becomes disadvantageous at higher temperatures when the flow stress decreases rapidly with increasing temperature. Strengthening methods to inhibit dislocation motion are required to improve carbide strength retention for working temperatures in the region of 1500°C. Hardening by the addition of <1% boron and the subsequent precipitation of borides in three-dimensional arrays by nucleation on $\{III\}$ planes has been studied by Venables[25] and shown by Williams[23] to increase the yield stress by a factor of five at 1600°C. Refining of grain size is also effective in strengthening polycrystalline carbides.

The effect of non-stoichiometry on the mechanical properties of carbides has been investigated for TiC[23] and TaC[26]. Non-stoichiometry in carbides is accommodated by vacancies in the carbon sublattice. In the case of TiC the flow stress decreases with deviation from stoichiometry, whereas in TaC the opposite effect is observed. There are several possible competing mechanisms here; (a) the simple dislocation interaction with vacancy mechanism raising the

flow stress. (b) The presence of vacancies lowering the Peierls stress by reducing the number of Me-C bonds and reducing the strength of Me-Me bonds. (c) The presence of vacancies aiding deformation at high temperature. The maximum Peierls stress has been observed[24] to occur in VC_{1-x} at sub-stoichiometric compositions at about V_6C_5 which is near to the maximum in melting point and to the composition at which 'bonding' 3-d states are just filled. Ordering of vacancies has a direct effect only on the ductile to brittle transition temperature[27], but may influence the flow stress by direct dislocation interaction and may have an indirect effect via modification of the Peierls stress when the structure is near the ideal co-ordination dictated by the electronic configuration mentioned above[24]. The effect of non-stoichiometry on flow stress in any particular case will be the net effect of the above mechanisms, and as none of these is quantitatively understood any firm deductions are difficult. Similar considerations must be expected to apply in the case of VSi_2.

Although the deformation mechanisms in carbides are not fully understood, high-strength engineering materials based on carbides are in production, and can exhibit good high temperature strength. The best carbide material to date is a VC-25 atomic percent TiC alloy which has a strength of 20 kg/mm^2 at 1800°C, and 1% ductility at 1000°C. The problem in using carbides at these elevated temperatures is their poor oxidation resistance.

1.5 Aims of the Present Work

The main objective of the research described in this thesis is the assessment of transition metal disilicides as high temperature structural materials, using VSi_2 as a model disilicide, and to interpret the observed mechanical deformation behaviour in terms of crystal structure, composition and defect structure. The research programme may be subdivided:-

(i) The growth of large, high-purity single crystals of VSi_2 with various compositions within the range of single phase stability.

(ii) A determination of the range of non-stoichiometry, structural mechanism for accommodation of non-stoichiometry and imperfection structure in Czochralski grown crystals.

(iii) A determination of the critical resolved sheer stress for slip on different systems with varying temperature and composition.

(iv) An interpretation of the observed macroscopic crystal plasticity in terms of crystal structure and slip dislocation structure.

(v) A critical evaluation of transition metal disilicides as high-temperature materials either in polycrystalline form or as one of the component phase in a composite material.

REFERENCES

(1) Kelly, A. In: Strong Solids. Clarendon Press (1966).
(2) Orowan, E. Rep. Prog. Phys. 12, 185 (1949).
(3) Frenkel, J. Z. phys. 37, 572 (1926).
(4) Groves, G. and Kelly, A. Phil. Mag. 8, 877 (1963).
(5) Hägg, G. Z. phys. Chem. (B) 12, 33 (1931).
(6) Goldschmidt, H. J. Interstitial Alloys. Butterworths (1967).
(7) Robins, D. A. and Jenkins, I. Acta Met. 3, 598 (1955).
(8) Voitevich, K. Porosh Met. 35, 43 (1974).
(9) Goldschmidt, H. J. Ibid. p.336 (1967).
(10) Efinov, Yn. V. Zh. Neorg. Khim. 8, 1522 (1963).
(11) Seeber, B. and Nickel, J. J. Phys. Stat. Sol (a) 15, 73 (1973).
(12) Nowotny, H. In: Electronic Structure and Alloy Chemistry of the Transition Elements. Wiley Interscience (1963).
(13) Aronson, B., Lundstrom, T. and Rundquist S. In: "Borides Silicides and Phosphides", Methuen (1965) ref. 44.
(14) Kurnakov, N. S. Proc. acad. sci. U.S.S.R. 26, 362 (1940).
(15) Schottkey, W. and Wagner, C. Z. phys. Chem. (Leipzig) B11, 163 (1930).
(16) Wadsley, A. D. In: Non-Stoichiometric Compounds. Acad. Press, N.Y. (1964).
(17) Magnéli, A. Acta Cryst. 6, 495 (1953).
(18) Ridder, R. de & Amelinckx, S. Mat. Res. Bul. 6, 1223 (1971).
(19) Westbrook, J. H. In: Mechanical Properties of Intermetallic Compounds, Wiley, N.Y. (1960).
(20) Lawley, A. In: Intermetallic Compounds (ed. Westbrook), N.Y. (1967).
(21) Stoloff, N. S. In: Strengthening Methods in Crystals. Elsevier (1971).
(22) Wood, D. L. and Westbrook, J. H. Trans A.I.M.E. 227, 771 (1963).
(23) Williams W. S. J. Appl. Phys. 35, 1329 (1964).
(24) Lye R.G., Hollox G.E. and Venables J.D. In: Anisotropy in Single Crystal Refractory Compounds, N.Y. (1968) p.445.
(25) Venables, J. D. Phil. Mag. 16, 873 (1967).
(26) Santoro, G. Trans A.I.M.E. 227, 1361 (1963).

CHAPTER 2

EXPERIMENTAL TECHNIQUES

2.1 Crystal Growth

2.1.1 Selection of Growth Technique

The broad categories of crystal growth are vapour phase, melt, flux and growth from the solid.

Vapour phase crystal growth consists of chemical transport of the components of the desired material as volatile compounds, usually metallo-organics or halides. These compounds are reduced in the presence of a suitable substrate, the elements combine, and crystals nucleate and grow on the substrate. This technique has the advantage of being performed at low temperatures compared with the melting point of the crystal concerned, and has been used[1] for the single crystal growth of many refractory compounds, including silicides.[2] In the present work the requirement for large crystals suitable for mechanical testing precludes the use of vapour phase growth, which yields crystals typically of the order of a few microns in thickness.

Growth from the solid by strain-annealing has been extensively used for metals[3]. Annealing of polycrystalline rods which have been given a critical amount of plastic strain, promotes the formation of large grains. Successive applications of this cycle can yield good single crystals. The application of this technique to inherently brittle solids such as silicides is problematical, and in any case the preparation of fully dense rods of closely-controlled composition of VSi_2 could only be done by direct reaction of

silicon and vanadium and subsequent lengthy homogenisation - a process which would be prone to contamination.

Flux growth, i.e. growth by precipitation from a super-saturated solution driven by evaporation or slow cooling, is not easily applied to transition metal compounds because of the problem of finding a flux with negligible solid solubility in the crystal. Control over crystal orientation and composition using this technique is very poor. Flux growth of VSi_2 was therefore discounted.

Melt growth is therefore the preferred technique for growing large, high-purity single crystals of VSi_2 with control over orientation and composition. The various techniques of growth from the melt differ only in the way the melt is contained and in the way the solid-liquid interface is driven to promote crystal growth. The technique used in any particular case is determined by two factors - the temperature required, and the containment of the melt without contamination from crucible or atmosphere and without loss of constituents.

The relatively high melting-point of VSi_2 ($1750^{o}C$) is above the limit for convenient application of resistance heating. The good electrical conductivity of disilicides indicates radio-frequency (r.f.) induction heating as a possible method. In this technique, an r.f. field is applied to a work coil closely surrounding the sample. Eddy currents induced in the sample cause resistive heating and eventually melting. With good coupling between coil and sample and sufficient r.f. power extremely high temperatures (up to $3000^{o}C$) may be reached. Induction heating has the additional

advantages of good mixing in the melt and easy adaption to working in vacuum or in a controlled atmosphere.

The problem of containing molten VSi_2 is severe. The reactivity of vanadium near its melting point is such that no crucible material is available which would not contaminate the melt at 1750°C. The vapour pressure of vanadium at this temperature is such that evaporation losses from the melt in vacuum are inevitable. A crucible free technique using r.f. induction melting in an inert atmosphere is therefore required.

A floating-zone r.f. melting method using pressed and sintered rods has been used extensively for the growth of single crystals of transition metal carbides and nitrides[4]. It would be feasible to grow silicides by this method, however, it does have disadvantages in the lengthy preparation of sintered rods with possible impurity contamination of particles with large surface area.

Another technique of r.f. melting without crucible contamination is that using cold-hearth levitation melting originally developed by Sterling[5]. Here the r.f. work coil surrounds a water-cooled boat of copper or silver which contains the samples. Eddy currents are induced in opposite directions in the boat and in the sample, causing levitation of the sample by repulsion. The sample then melts by conventional r.f.-melting without contact with the boat, which is in any case efficiently water-cooled. In this way crucible contamination is minimised. A schematic diagram of the basic cold-hearth apparatus is shown in Fig. 2.1. This apparatus has been used occasionally in this research for preliminary preparation of alloys. A Czochralski

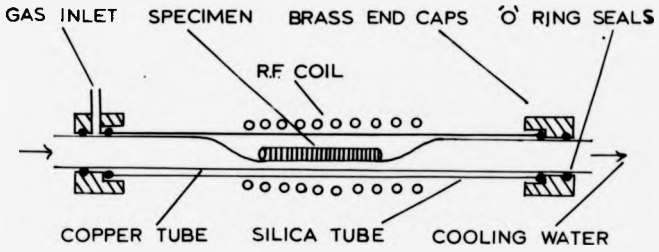

Fig. 2.1 Cold-hearth levitation melting apparatus

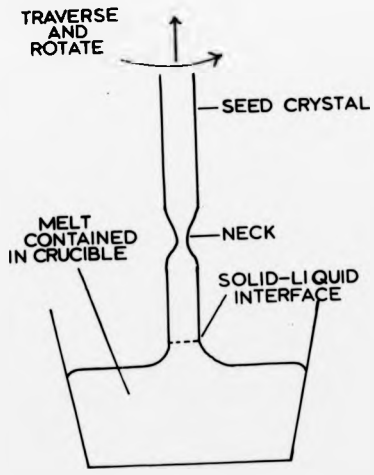

Fig. 2.2 Czochralski crystal growth

crystal growth technique using the cold boat principle has been used to grow the crystals studied in this thesis. The principles of the Czochralski method are shown in Fig. 2.2. A seed crystal (or wire) is lowered into the melt, allowed to melt back and stabilise, and is withdrawn gradually from the melt, rotating at a constant speed. This is equivalent to moving the solid-liquid interface through a temperature gradient, promoting crystal growth. The advantages of the Czochralski technique over the floating zone method outlined above are the greater stability of the growth process, greater control available, increased visibility of the melt during growth, choice of orientation of crystal by cutting an appropriate seed, and above all, ease of preparation of starting materials.

2.1.2 Crystal Growth Apparatus

The principle of cold hearth levitation melting has been outlined above. For Czochralski crystal growth the requirement is for a stable melt of approximately 30 cm^3 (i.e. 100 grams for VSi_2) held in a radially uniform temperature distribution, and with access from the top for the seed crystal to be pulled away vertically. These requirements are met by the cold crucible[+] shown in Figs. 2.3(a), (b) and (c). This crucible has been machined from a solid bar of copper and consists of a basket-shaped container with a capacity of about 50 cm^3 made up of an axially symmetric array of individually water-cooled segments. Each segment is electrically isolated in

[+]Metals Research Ltd. HCC50

crystal growth technique using the cold boat principle has been used to grow the crystals studied in this thesis. The principles of the Czochralski method are shown in Fig. 2.2. A seed crystal (or wire) is lowered into the melt, allowed to melt back and stabilise, and is withdrawn gradually from the melt, rotating at a constant speed. This is equivalent to moving the solid-liquid interface through a temperature gradient, promoting crystal growth. The advantages of the Czochralski technique over the floating zone method outlined above are the greater stability of the growth process, greater control available, increased visibility of the melt during growth, choice of orientation of crystal by cutting an appropriate seed, and above all, ease of preparation of starting materials.

2.1.2 Crystal Growth Apparatus

The principle of cold hearth levitation melting has been outlined above. For Czochralski crystal growth the requirement is for a stable melt of approximately 30 cm^3 (i.e. 100 grams for VSi_2) held in a radially uniform temperature distribution, and with access from the top for the seed crystal to be pulled away vertically. These requirements are met by the cold crucible[+] shown in Figs. 2.3(a), (b) and (c). This crucible has been machined from a solid bar of copper and consists of a basket-shaped container with a capacity of about 50 cm^3 made up of an axially symmetric array of individually water-cooled segments. Each segment is electrically isolated in

[+]Metals Research Ltd. HCC50

Fig. 2.3 Cold crucible

the r.f. field applied by a surrounding work coil, and acts independently as a transformer, hence the r.f. coupling and magnetic levitation are very efficient, enabling relatively low power generators to be used. The crucible is rhodium-plated.

For each crystal growth, the cold crucible was mounted as shown in Fig . 2.4 in the crystal growth apparatus previously described by Billingham[6]. This consists of a stainless steel growth chamber containing ports for the r.f. coil input and for viewing the crucible. The cold crucible was mounted in a stainless steel baseplate using a sliding O-ring seal as shown. The r.f. work coil was wound as close as possible to the crucible with the maximum number of turns to optimise magnetic coupling and reduce the power requirements. A 30 kW r.f. generator working at 470 kHz was used with a 67 kVA saturable core reactor allowing close control of the power supplied and stabilising the output with respect to input voltage fluctuations, both of critical importance during crystal growth. Similarly, the lead screws which rotate and pull the seed crystal are both driven by variable speed motors with stabilised outputs. The seed could be rotated at from 0.5 to 360 revs/min. and traversed at 6.0 to 600 mm/hour with, in addition, a special high speed for rapid positioning of the seed crystal prior to growth.

The growth chamber is designed for use at up to 20 atmospheres pressure if required, and is equipped with a set of blow off valves at 5, 10 and 20 atmospheres, providing a means of maintaining a constant chamber pressure. In the

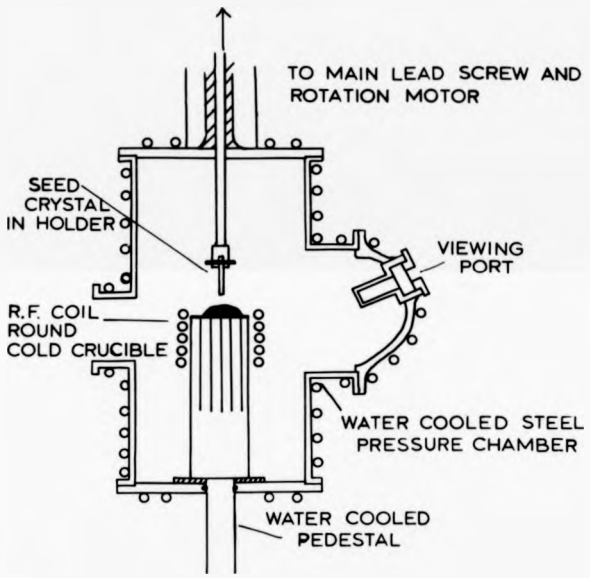

Fig. 2.4 Crystal growth chamber

present work, a pressure of 10 atmospheres of helium was used. Helium was selected because of its high ionisation potential relative to argon. The value of 10 atmospheres was chosen because it has been shown[7] that at or above this pressure convection losses are minimised. The chamber and cold crucible have separate water-cooling. Water-cooling on the cold crucible is critical and a minimum flow of 4 gals/minute was maintained.

The viewing port consists of a 'spectrosil' grade silica window, 2.5 cm thick with special seals for high pressure work. Good visibility during crystal growth is essential and to ensure ease of cleaning after each run, a second silica window, easily removable, was placed on the inner side of the port.

The r.f. coil leads entered the chamber through O-ring seals in a tufnol-sindanyo insert. Arcing between the leads can occur across the surface of this insert due to accumulation of a conducting film during crystal growth. To avoid this, the first few centimetres of the leads inside the chamber were coated with heat resistant silicone rubber.

2.1.3 Czochralski Growth Procedure

The materials used were vanadium turnings >99.8% pure (purchased from either Koch Light Ltd., Bucks., or from Metals Research Ltd., Herts.) and silicon granules of 99.9999% purity (Koch Light Ltd., Bucks.).

The starting materials were weighed out in the proportions to give the desired disilicide composition, and melted in the cold crucible apparatus described above. A bulk melt of about 100 gms of VSi_2 was required to give the good visibility of

solid-liquid interface required in the early stages of crystal growth. To obtain a melt of this size required pre-melting of the alloy in lots of about 30 gms, and subsequent melting of three 30 gm boules together.

For each pre-melting run the procedure adopted was as follows. The crystal growth chamber was flushed out three times with high purity helium, and helium was pumped through the chamber for 30 minutes. The chamber was then filled to 10 atmospheres of helium and the blow-off tap opened. After ensuring an adequate water flow through crucible and chamber the r.f. power was turned on and slowly increased until the V-Si reaction commenced. Since the reaction to form VSi_2 is exothermic, once the reaction started the power was reduced. The melt was held above the melting point for 15 minutes to allow homogenisation. The power was then slowly reduced to allow formation of a fully dense boule to obtain maximum amount of material in the crucible for crystal growth.

For single crystal growth, the maximum amount of pre-melted material of the desired composition was placed in the crucible, melted and held for 15 minutes to allow homogenisation. Figure 2.5(a) shows the complete charge, molten, prior to crystal growth. The melt has the appearance of a pear-shaped drop, and is levitated considerably from the crucible walls. The drop is stable at temperatures above the melting point, and at these temperatures there is considerable agitation in the melt.

The seed crystal used for Czochralski crystal growth was a crystal of VSi_2 cut using a diamond saw to approximately

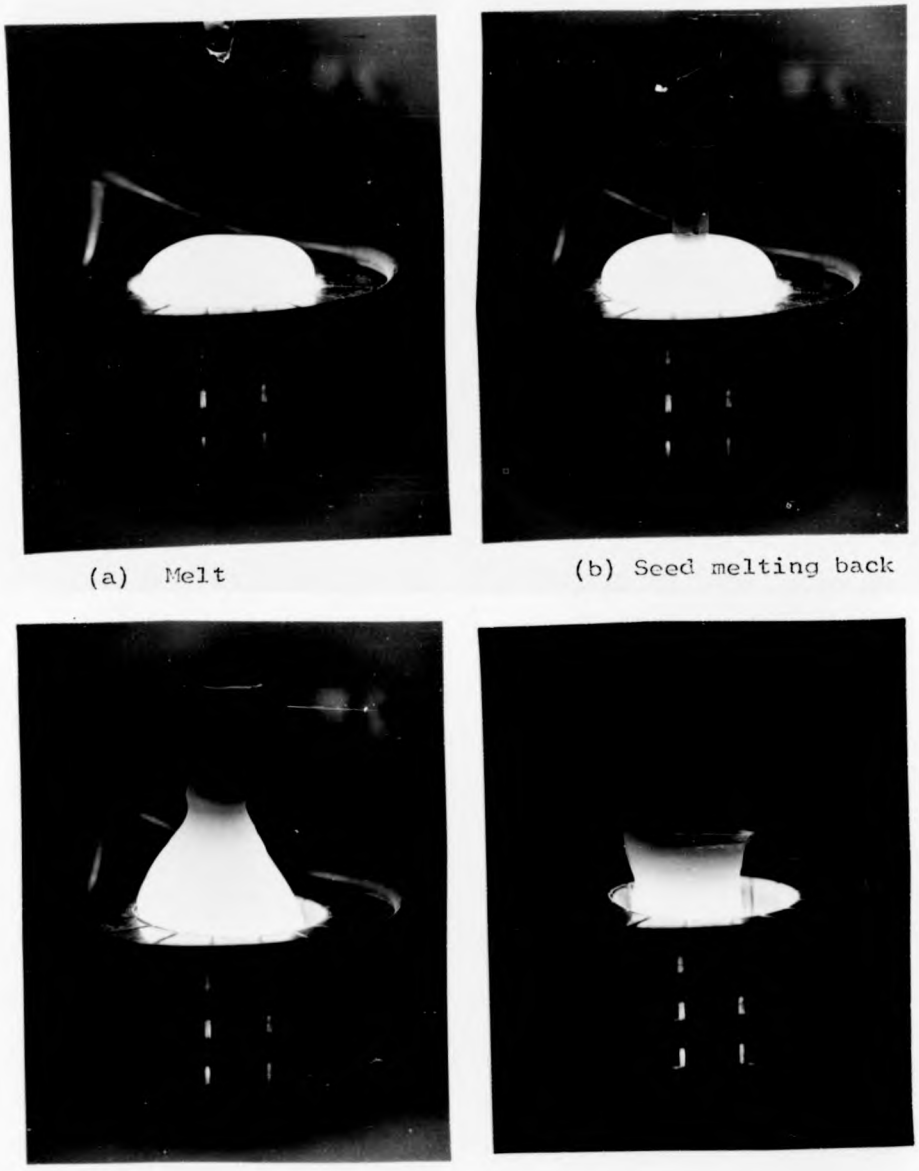

(a) Melt (b) Seed melting back

(c) Early stage of growth (d) Later stage

Fig. 2.5 Single crystal growth

20 x 3 x 3 mm mechanically ground followed by chemical polishing. The seed was held in a stainless steel clamp held in the pull-rod. The seed crystal was lowered into the melt and allowed to remain stationary until it had melted to form a smooth meniscus (Fig. 2.5(b))

Growth was then initiated by withdrawing the seed from the melt and increasing the melt temperature to produce an initial reduction in the diameter of the crystal (Fig. 2.5(c)). In practice the narrowest neck which could be achieved was about 4 mm diameter. At this stage, by a combination of very gradual reduction of applied power and of seed withdrawal rate the diameter of the pulled crystal was increased. To facilitate the cutting of mechanical test specimens of various orientations the diameter of the crystal should be as large as possible. The most convenient size of crystal was found to be 1.5-2.0 cm. Once a diameter of this order had been achieved conditions were adjusted to maintain this diameter constant. The crystals grown were usually 20 cms long and weighed about 80 gms. The intermediate and final stages of crystal growth are shown in Figs. 2.5(d) and (e), and the final bulk crystal in 2.5(f). A typical growth rate was 1 cm/hour average, say 1.5 cm/hour in the early stages and 0.3 cm/hour finally. Rotation of the crystal was attempted, but it was found that no improvement in crystal quality was obtained, no doubt because of the extremely good axial symmetry of the temperature distribution.

Fig. 2.5 (e) Final stages of growth

x2

Fig. 2.5 (f) Final crystal

2.2 Microstructural Analysis

2.2.1 Optical Metallography

Extensive use of optical metallography has been made in this research, hence a brief account of the preparation of sections for optical microscopy will be given.

Crystal cutting of VSi_2 is difficult because of the inherent hardness and brittleness of the material. Mechanised cutting, i.e. diamond cutting would induce damage to such a degree as to affect particularly the mechanised testing to an unacceptable level. The good electrical conductivity of VSi_2 enables spark erosion to be used, and this was the technique used throughout the present work for preparing the crystals for optical and electron microscopy and for mechanical testing. Spark erosion was carried out using a Metals Research Servomet spark machine.

In the case of sections for optical metallography, a modified wire-cutter was used to obtain slices from the bulk crystal. Slices for optical microscopy were cut using the middle ranges of spark energy (range 4 or 5). The slices were mounted in "specifix" plastic mounts, and mechanically polished using successively 220, 440 and 600 silicon carbide papers followed by 6, 1 and $^1/_4$ micron diamond impregnated polishing cloths. The polished speciments were then lightly etched using H_2O:HF:HNO_3 in 50:1:1 proportions.

The optical microscope used was a Zeiss Ultraphot II equipped for examination in reflection using polarised light, interference contrast and dark field microscopy. For low magnification work, less than x10 special wide angle objectives were used.

2.2.2 Electron Microscopy

All the electron microscopy reported in this thesis was performed using a JEM 200 microscope operating at 200 kV.

For 200 kV electron transparency, sample thicknesses of the order of 3000-4000Å are prepared for VSi_2. These thin sections were prepared by the following technique. A slice about 0.5 mm was spark machined from the bulk crystal using the wire cutter as above, but in this case, to minimise induced defects the lowest energy range (6 or 7) was used. Discs 3 mm diameter were spark cut from this thin section using a cylindrical brass tool, again at the lowest energy range. These discs were polished using 600 grit silicon carbide and 6 micron diamond, and were mounted in a P.T.F.E. holder for electrothinning. Some difficulty was encountered in achieving satisfactory electropolishing conditions for VSi_2. The electrolyte recommended[8] for vanadium, methanol with 25% sulphuric acid, with a graphite cathode at 20 volts was found to give very poor results for the disilicide, probably because of the formation of an inert oxide layer on the surface. The conditions found to give best results were methanol with 5% sulphuric and 1% hydrofluoric acid using a nickel cathode and a potential of 35 volts. Under these conditions the disc was polished to perforation. Perforation was detected by focussing a lamp on to one side of the disc, and observing the other side using a telescope. At the first sign of perforation the current was switched off, the specimen removed and rinsed immediately in analar methanol to ensure the absence of a contaminating surface

film and to prevent chemical reaction with the electrolyte. This procedure gave satisfactory electron transparent areas. A significant improvement could be achieved by giving the perforated disc a final treatment by ion-beam sputtering. This had the dual purpose of increasing the thin area and achieving a high degree of cleanliness of the specimen. Optimum conditions for ion-beam sputtering were found to be 6 keV argon ions, 4 mA current with the specimen inclined at 45° to the ion beam and rotated continuously. An ion-beam treatment of about 5 hours was found to give a substantial improvement. This treatment was given to most discs used in the present work. The finally thinned discs could be mounted directly in the electron microscope specimen holder without the use of support grids because of the robust outer rim remaining on the discs. The electropolished discs could be stored in a vacuum desiccator without surface contamination.

2.3. Single Crystal Deformation

2.3.1 Apparatus

Compression testing was chosen as the technique which would give most data on the deformation of VSi_2 crystals. Tensile testing of brittle materials such as VSi_2 is very difficult because of the problems of machining test-pieces and of gripping the specimen in tension. Three-point bending gives a non-homogeneous stress pattern and much less information than compression. Indentation hardness could give limited information on operative slip systems, but would not give information on the bulk material under stress or provide material deformed uniformly for subsequent analysis by transmission electron microscopy.

All compression testing was performed with a 5000 kgm maximum capacity Floor Model Instron Testing Machine fitted with special low strain rate and fast recorder modifications for ceramics work, and with pushbutton selector control for instantaneous crosshead speed changes.

For high-temperature testing a silicon carbide muffle element was used (Morganite Electroheat Ltd.). This open-ended element had a hot-zone 10 cm long and a diameter of 30 mm which was ideal for accommodating a compression test specimen and push-rods. This element was mounted in a furnace with a water-cooled casing suspended from the crosshead of the test machine (Fig. 2.6). The power supply and temperature controller used was a stepless controller with thyristor output (Eurotherm Ltd.) rated at 25 amps output. A Pt.-Pt.13% Rh thermocouple was placed adjacent to the compression specimen. This furnace could be used at temperatures up to 1550^{o}C with temperature control to $\pm$ $^{1}/_{4}{}^{o}$C.

The compression anvils used were rods of recrystallised alumina (Thermal Syndicate Ltd.) with their ends ground parallel using a diamond impregnated wheel. The rods were held in good axial alignment by water-cooled stainless-steel collets which were screwed directly into the crosshead and the compression table (Fig. 2.7).

The output data from each test is in the form of a plot of total stress (as measured by the compression load-cell) against total strain, i.e. the product of the selected crosshead speed and time. For small strains this can be regarded as a true stress-strain curve, see Appendix to Chapter 4, page 58.

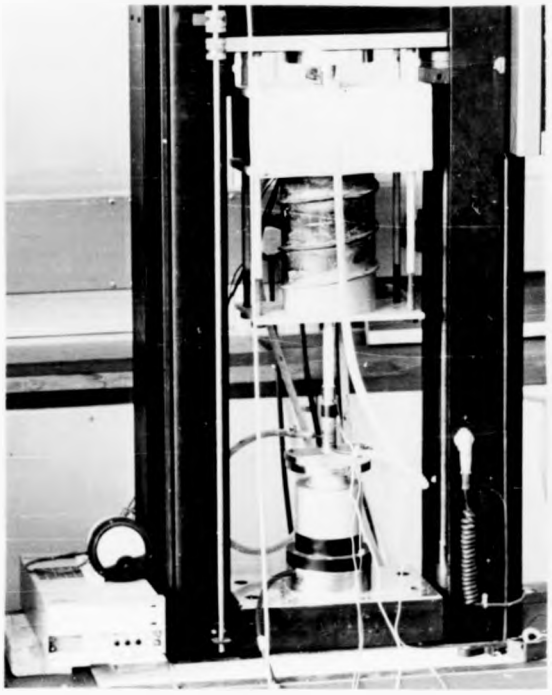

Fig. 2.6 Compression testing apparatus

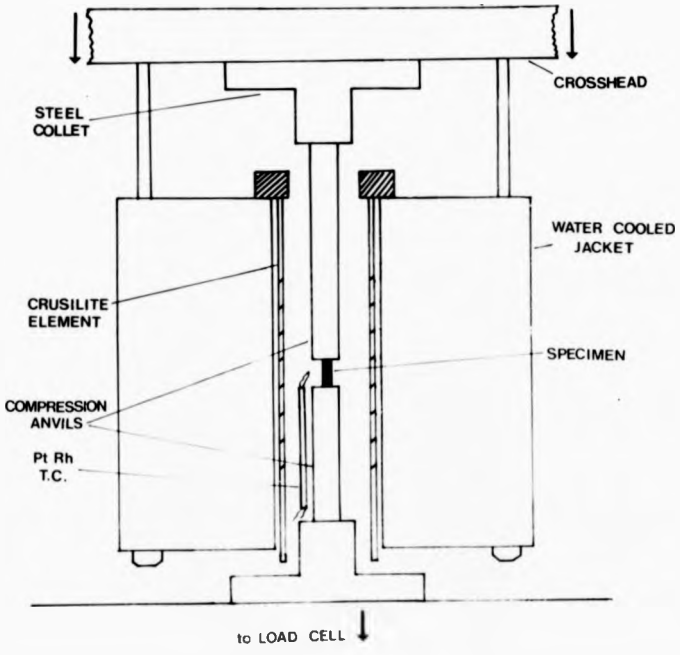

Fig. 2.7 Compression testing apparatus

2.3.2 Specimen Preparation and Test Procedure

Selection of crystal orientations for compression testing will be discussed in Chapter 4, and the orientation of as-grown crystals in Chapter 3. For compression testing, rectangular bars 9 x 3 x 3 mm were spark machined from the orientated crystal using the wire cutter on range 7. These dimensions were chosen to satisfy the length:breadth $\geq$ 3:1 criterion for homogeneous strain in compression, and to obtain a sufficient number of compression specimens of different orientations from each crystal. The main problem in specimen preparation was to ensure that opposite faces of the specimen were parallel, and adjacent faces perpendicular. Parallelism of the end faces is particularly critical to avoid localised mis-orientation and stress raising. To achieve the desired accuracy, the spark-machined bar was mounted in a stainless steel polishing jig for the final mechanical polishing to $^{1}/_{4}$ micron diamond. The planing tool attachment of the spark machine was used on range 7 to prepare the end faces of the specimen, which, in this case, was mounted on a table which itself had been previously planed. The whole specimen was then given a short electropolish under the same conditions as for electron microscopy.

To ensure the validity of direct comparison of tests with variations of temperature, strain-rate and composition, the following procedure was adopted for each test.

The orientated compression specimen, prepared as described above, was lightly tacked at one corner on to the lower alumina anvil using an adhesive which would burn off

prior to the test. The crosshead upper anvil, and attached furnace were lowered, and the upper anvil brought into contact with the specimen using the manual crosshead positioning facility. The furnace temperature was increased slowly (300°C/hour) to the test temperature to avoid thermal shock in the compression specimen and in the anvils. Thermal expansion of machine, anvils and specimen was accommodated using the load cycling facility to maintain the load on the specimen between pre-set limits of 1 and 2 kgm. When the test temperature had been reached, the apparatus was left in this load cycling mode for 1 hour to ensure complete stability of the apparatus at the control temperature. The compression test was commenced at the selected strain-rate and monitored on the chart recorder.

The strain-rate used for all experiments other than the strain-rate dependence tests was 0.005 cm/min. The range of strain rates available was 0.0005 to 5 cms/min. Load cells with ranges from 1 to 5000 kgm full-scale deflection were available. A suitable load cell was selected for each test taking account of specimen orientation, test temperature, and strain rate. The recorder chart speed was selected to facilitate analysis of the stress-strain curves obtained, and was usually 0.5 cm/min.

Each test was concluded at an appropriate strain-level, usually the maximum strain possible leaving the specimen intact except for strain-rate variation experiments or for electron microscopy specimens at different strains. The furnace was then cooled as quickly as possible. Here a

compromise had to be made between possible cracking of anvils and specimen and attempting to "quench-in" the dislocation structure at the conclusion of the test rather than allow possible modification by, for example, climb during slow cooling.

After each test the anvils were checked for damage and alignment prior to the next test.

REFERENCES

(1) Nagasawa, K. Jap. J. App. Phys. 9, 407 (1970).

(2) Wandji, E. Comptes Rend. C, 267, 1587 (1968).

(3) Aust, K. T. In: Art and Science of Growing Crystals, Wiley, N. Y. (1963).

(4) Billingham, J., Bell, P. S. and Lewis, M. A. J. Cryst. Growth, 13/14, 693 (1972).

(5) Sterling, H. F. and Warren, R. W. Metallurgia 67, 2 (1963).

(6) Billingham, J. Ph.D. Thesis, Warwick University (1971).

(7) Chesswas, M., Cockayne, D., Hurle, D., Jakeman, K. and Mullin, J. B. J. Crystal Growth 11, 225 (1971).

(8) Edington, J. W. and Smallman, R. E. J. Aust. Inst. Metals 8, 8 (1963).

CHAPTER 3

CRYSTAL CHARACTERISATION

3.1 Non-Stoichiometry

3.1.1 Composition Limits of VSi_{2-X}

The importance of deviation from stoichiometry in the work described in this thesis has been emphasised above. From the phase diagram (Fig. 1.2) VSi_2 is estimated to have a broad range of homogeneity which has not previously been investigated in detail. A necessary preliminary to a study of the influence of non-stoichiometry on plasticity of vanadium disilicide is a determination of the relevant phase boundaries of VSi_2. This was carried out as follows.

As a rough estimate of the composition limits of VSi_2 small samples of the order of 5 gms were prepared using the basic r.f. levitation melting apparatus (Fig. 2.1). Samples were prepared of compositions from $VSi_{1.50}$ to $VSi_{2.20}$ and each was examined using standard Debye-Scherrer X-ray powder diffraction techniques and optical metallography to determine the single phase compositions and to identify the second phases present outside the single-phase region. From these experiments the homogeneity range of VSi_{2-X} was found to be $VSi_{1.70}$ to $VSi_{1.95}$, i.e. 63.0% atomic to 66.2% atomic silicon. A discussion of the phase equilibria near VSi_2 will be given in section 3.3 below.

Single crystals were grown as described in section 2.1 of compositions $VSi_{1.70}$, $VSi_{1.80}$, $VSi_{1.85}$, $VSi_{1.90}$ and $VSi_{1.95}$.

A programme of annealing and quenching experiments was carried out on specimens cut from the as-grown crystals to obtain more accurate information on the phase boundaries of VSi_2. The approximate homogeneity range determined by melting of small boules and subsequent rapid cooling yielded no information on the variation of homogeneity range with temperature. Lengthy (1000 hour) anneals at temperatures in the range 600-1100°C and quenches in air from these temperatures were performed for each composition, and again X-ray and optical methods were used to establish the appearance of any second phase. Figure 3.1 shows the results of this programme, and these experimental points together with data on the liquidus near VSi_2[1] have been used to draw the phase boundaries of VSi_{2-X} (Fig. 3.1). Comparison of Figs. 1.2 and 3.1 shows that the estimate of homogeneity of VSi_2 of Kieffer and Benesovsky[1] is in reasonable agreement with the present work.

3.1.2 Structural Accommodation of Non-Stoichiometry

It is important to establish the mode of accommodation in VSi_{2-X} of the deviations from stoichiometry observed in 3.1.1 above in order to interpret the influence of non-stoichiometry on plasticity in terms of deformation mechanisms. The possible modes of accommodation were outlined in section 1.3.2 above. In the present case, excess V atoms may be accommodated by (a) interstitial V atoms (b) Si vacancies or (c) substitution of V on Si sites.

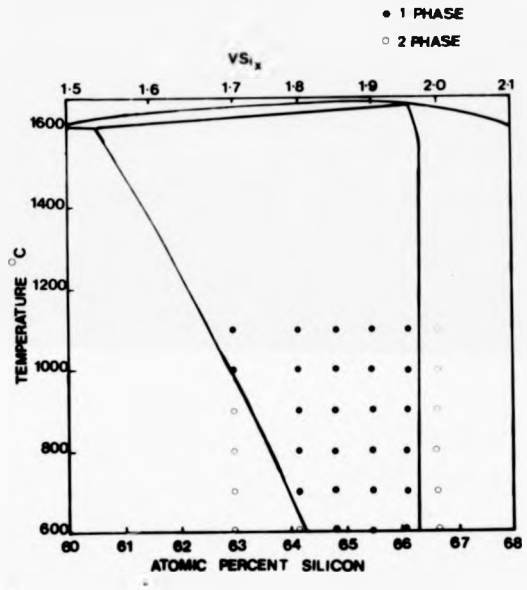

FIG. 3.1 Phase boundaries of VSi_{2-x}

Calculation of the octahedral interstice size (the largest interstice) in VSi_2 using the method of Mayer et al.[2] and the approximate bond lengths given by Robins and Jenkins[3] gives a value of 2.1Å[4]. Thus interstitial accommodation of excess V atoms can be ruled out. To distinguish between mechanisms (b) and (c) a series of lattice parameter measurements using Hägg-Guinier focussing camera X-ray powder diffraction and pyenometric density determinations were performed on the as-grown crystals. The results of these experiments are shown in Table 3.1. Also included here are density calculations assuming accommodation of non-stoichiometry by (a) V substitution, $V_y Si_{2-y}$ and (b) Si vacancies, VSi_x for each composition. The density results show that Si vacancies is the more likely mechanism operating. The evidence is not conclusive, but the tendency towards density decrease with departure from stoichiometry is there. The lattice parameter changes observed are rather inconclusive. The anticipated decrease of a parameter with Si vacancies is not observed unequivocally. However, the evidence of these experiments indicates that accommodation of non-stoichiometry in VSi_{2-x} is by vacant Si sites.

3.2 Composition and Impurity Analysis

In view of the importance of non-stoichiometry in the work described in this thesis, it is essential to characterise the composition and impurity content of the as-grown crystals.

COMPOSITION		LATTICE PARAMETERS (experimental)		D E N S I T Y (gm cm^{-3})		
VSi_x	atomic % Si	a Å	c Å	experiment	(a) VSi_{2-Y}	(b) $V Si_X$
$VSi_{1.7}$	63.0	4.63	6.39	4.11	4.52	4.07
$VSi_{1.8}$	64.2	4.61	6.40	4.25	4.48	4.18
$VSi_{1.85}$	65.0	4.62	6.38	4.26	4.47	4.24
$VSi_{1.9}$	65.6	4.57	6.37	4.35	4.46	4.30
$VSi_{1.95}$	66.2	4.56	6.39	4.38	4.42	4.34

TABLE 3.1 Experimental values of density and lattice parameters and calculated densities

Specimens were sent for analysis to Johnson Matthey Ltd. and the results are shown in Tables 3.2 and 3.3.

Macroscopic segregation in the as-grown crystals was checked by determining the Si content in sections taken from the top, middle and lower parts of the crystal. The results (Table 3.2) show that the Si content is highest at the top of the crystal, i.e. that part which solidified first. The middle portion of the crystal has a lower Si content which is confirmed as being the nominal composition of the crystal. The lower portion has a still lower Si content. This segregation can be readily interpreted in terms of the theory of "normal freezing". The Si distribution in the crystal is typical of the case of normal freezing (e.g. crystal growth from the melt) in which the segregation coefficient for Si in VSi_2 is >1, under conditions of zero mixing in the solid and limited mixing in the liquid. Under such conditions a silicon deficient layer of liquid is maintained at the solid-liquid interface, and the silicon concentration, high in the initial growth stages reaches a constant level close to the nominal melt composition in the central part and finally a silicon deficient portion solidifies.

This segregation also gives information on the phase diagram, in particular on the liquidus near VSi_2. The fact that the first portion of the crystal to solidify has a composition near the upper limit of the homogeneity range means that the maximum of the liquidus lies at the Si-rich end of the VSi_2 phase-field.

NOMINAL COMPOSITION		PORTION OF CRYSTAL	EXPERIMENTAL COMPOSITION % Si
VSi_x	wt. % Si		
$VSi_{1.90}$	49.0	Middle	49.2
$VSi_{1.80}$	48.0	Middle	48.0
$VSi_{1.70}$	47.0	Top	48.1
$VSi_{1.70}$	47.0	Middle	47.1
$VSi_{1.70}$	47.0	Bottom	47.0

TABLE 3.2 Chemical analysis of as-grown crystals

ELEMENT	QUANTITY PRESENT p.p.m.
Aluminium	200
Calcium	5
Chromium	20
Copper	100
Iron	100
Magnesium	1
Manganese	10
Molybdenum	70
Nickel	70

Elements sought but not detected:-

Ag, As, Au, B, Ba, Be, Bi, Cd, Co, Cs, Ga, Ge, Hf, Hg, In, Ir, K, Li, Na, Nb, Nl, Os, P, Pb, Pd, Pt, Rb, Re, Rh, Ru, Sb, Se, Sn, Sr, Ta, Te, Ti, Tl, W, Zn, Zr.

TABLE 3.3 Spectrographic analysis of as-grown crystal

The other results in Table 3.2 are on samples cut from the middle portions of crystals of other nominal compositions and in each case confirm that these compositions are close to the nominal composition of the bulk melt.

In all the characterisation of phases and mechanical deformation work reported in this thesis, the samples were cut from the middle portions of the as-grown crystals, and the above results justify the assumption made that the crystal composition can be taken as the initial melt composition.

Table 3.3 shows the results of a spectrographic analysis of a specimen cut from a typical crystal (middle portion) - the one on which the silicon segregation analysis was performed. The results show that impurity levels are acceptably low, justifying the assumption that impurity effects on phase equilibria and on bulk mechanical properties are negligible. The absence of copper and rhodium in high concentrations in the as-grown crystals confirms that there was no contamination of the melt by the cold-crucible used in the crystal growth technique.

3.3 Phase Equilibria Near VSi_2

In addition to the determination of the phase boundaries of the disilicide described in 3.1.1 above, the other phases present near VSi_2 were studied in the course of the annealing experiments to establish the V-Si phase diagram in this region.

On the silicon-rich side of VSi_2, i.e. at compositions containing greater than 66.2% atomic silicon, a second phase was observed on optical examination of annealed specimens.

X-ray analysis suggested that this phase was elemental silicon, and optical examination using polarised light showed that the second phase particles had the pinkish colour characteristic of silicon. The presence of silicon was confirmed by transmission electron microscopy on ion-beam thinned specimens in which silicon particles were identified by electron diffraction.

The vanadium-rich side of the disilicide phase was examined in the same way as above, and the results proved to be less straightforward. Crystals with compositions close to the V-rich boundary of VSi_{2-X} were found to contain hexagonal particles which thinned preferentially on electro-polishing which made the preparation of specimens suitable for phase identification very difficult. It was assumed at first that the second phase particles were V_5Si_3, the next reported phase on the V-rich side, in very low volume fraction near the phase boundary, particularly as V_5Si_3 had been confirmed by X-ray diffraction as being present in the V-rich specimens prepared in the preliminary determination of homogeneity range. Ion-beam thinning enabled electron diffraction patterns of these second-phase particles to be recorded in a few cases. These patterns could not be indexed as any known phase in the V-Si system. As shown in 3.2 above impurity phases can be discounted. The possibilities which had to be checked in the course of the annealing and quenching experiments were a low temperature eutectoidal decomposition of $VSi_2 \longrightarrow X+Si$ where X is the unknown phase, or the existence of a new V-Si phase between V_5Si_3 and VSi_2, possibly

incongruently melting at a low temperature.

The possibility of eutectoidal decomposition of VSi_2 was checked by low temperature anneals (600°C for 1000 hours). Such a heat treatment should appreciably increase the amount of second phase present by progression of the eutectoidal decomposition towards the equilibrium situation of complete dissociation of VSi_2. No increase of second phase was observed as a result of these low-temperature anneals.

The experimental evidence is consistent with the existence of a "new" phase between V_5Si_3 and VSi_2. There have been two recent announcements of "new" phases in the V-Si system in the V_5Si_3—VSi_2 range.

Hallais and co-workers[5] report the existence of a V_6Si_5 phase with orthorhombic unit cell of dimensions

$$a = 15.95\text{Å}, \quad b = 7.45\text{Å}, \quad c = 4.82\text{Å},$$

and closely related to the V_5Si_3 structure with a different stacking sequence only.

Kocherzhinskii et al.(1973)[6] report on V_5Si_4 phase, melting incongruently at 1670°C with a eutectic point at 1640°C with VSi_2.

X-ray data are given for the new phase in both cases. A detailed comparison of the results of these workers is given in Table 3.4. This suggests strongly that the same phase has been observed in both cases. The French work[5] gives a complete unit cell determination, and their assignment of the formula V_6Si_5 is to be preferred to the Russian's estimate[6] of V_5Si_4.

d (obs.)Å (Hallais)	Indices (Hallais)	$\sin^2\theta$ (observed) Hallais	Kocherzhinskii	Electron Diffraction d(obs)	hkl
3.398	220	0.11374			
2.854	411	0.16110		7.97Å	200
2.429	002	0.22216	0.22270	6.83	110
2.263	330	0.25591	0.25105	5.53	210
2.228	611	0.26393	0.26434	5.01	300
2.182	710	0.27524		4.82	001
2.174	521	0.27725	0.27770		
2.170	620	0.27827	0.27940		
2.142	231	0.28574	0.28569		
2.120	312	0.29173	0.29330		
2.074	402	0.30443	0.31027		
2.039	022	0.31523	0.31756		
1.995	800	0.32904	0.32817		
1.973	222	0.33590	0.33063		
1.969	530	0.33817	0.33986		
1.942	431	0.34744	0.35000		
1.875	040	0.37268			
1.868	512	0.37400	0.37430		
1.793	422	0.39760	0.39808		
1.770	602	0.40723	0.40957		
1.727	811	0.40790			
	141	0.43335	0.43733		

TABLE 3.4 X-ray and electron diffraction data on V_6Si_5

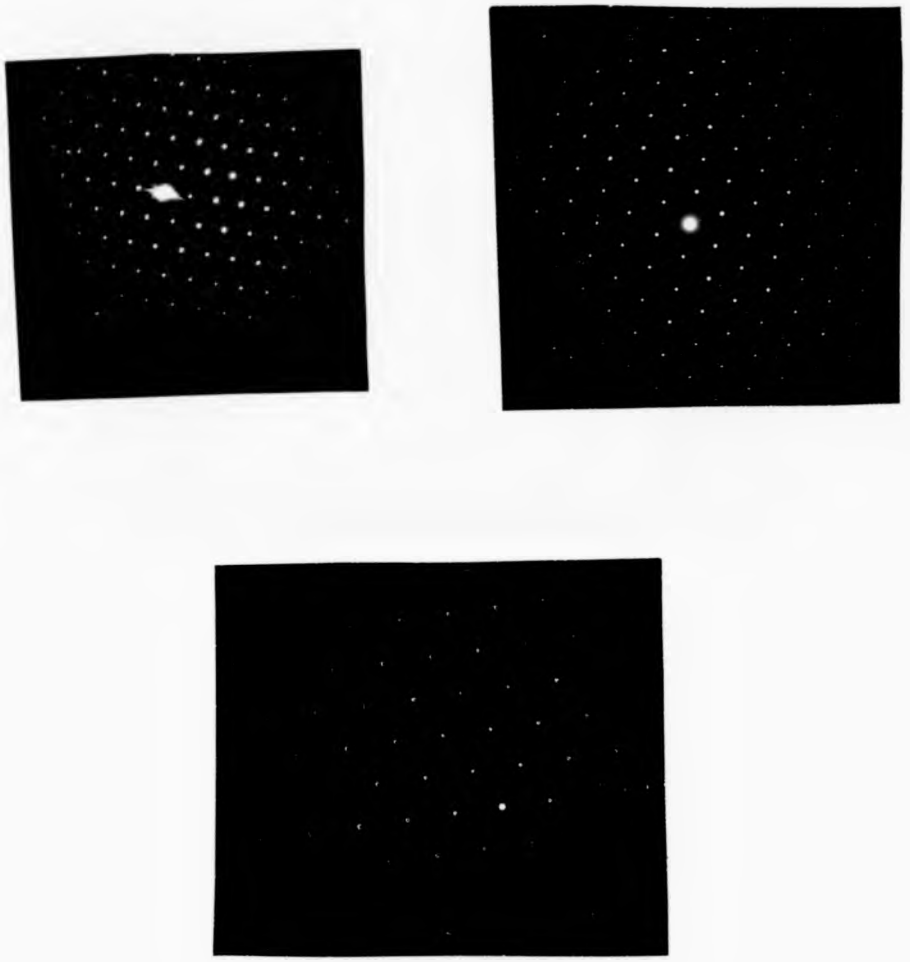

FIG. 3.2 Electron diffraction patterns from "new" phase.
d-spacings obtained are those quoted in Table 3.4

The inter-planar spacings found by electron diffraction from second phase particles in the present work are included in Table 3.4, and it may be seen that they are consistent with the X-ray data on V_6Si_5. The reciprocal lattice sections shown in Fig. 3.2. may be indexed on the orthorhombic unit cell. This is convincing evidence that the second phase observed here is the V_6Si_5 phase reported by Hallais[5].

The V-Si phase diagram given[6] by Kocherzhinski et al. is not consistent with the observation in the present work of V_5Si_3 as the second phase in V-rich specimens annealed at high temperatures. It is proposed that the incongruent melting point of the new phase is lower than that proposed in[6]. A proposed new phase diagram for the V-Si system is given in Fig. 3.3. This includes V_6Si_5. The incongruent melting temperature of V_6Si_5 is an estimate from the annealing experiments. Figure 3.3 also includes recent work on the V-Si system in the region of V_3Si by Seeber[7].

3.4 Crystal Perfection and Orientation Analysis

The single crystal nature of the as-grown crystal was confirmed by optical examination of a section cut perpendicular to the growth axis near the necked-down portion of the crystal. Once confirmed as a single crystal the as-grown crystal was mounted on a goniometer adapted for use either on the spark machine or on a standard Philips X-ray set.

A series of back reflection Laue photographs was taken initially with the X-rays incident in the growth direction. A typical Laue photograph is shown in Fig. 3.4. These Laue

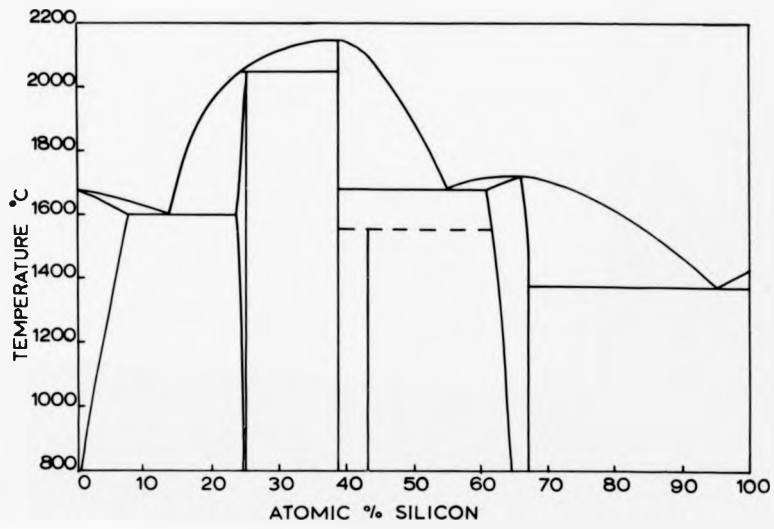

Fig. 3.3 Proposed new V-Si phase diagram

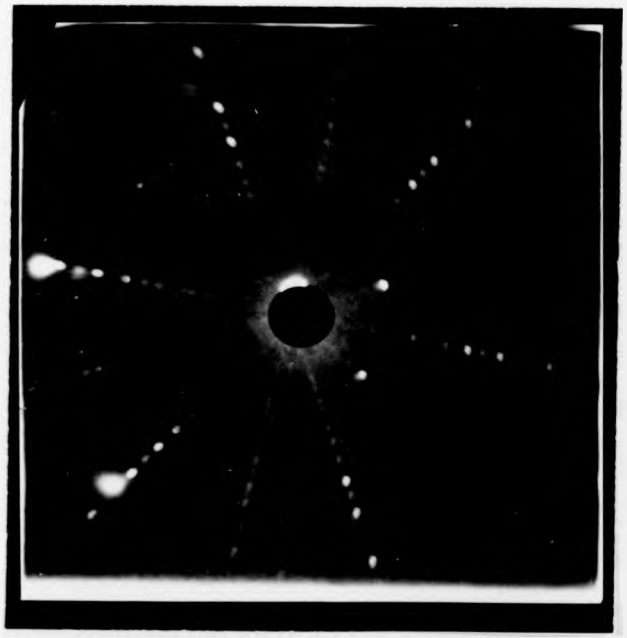

Fig. 3.4 Typical back-reflection Laue photograph

photographs are a useful confirmation of the single crystal, in addition to giving the orientation of the crystal with respect to the growth axis.

It was found that in most cases the growth direction was close to the c-axis, i.e. within 5^{o}, and in all cases was within 15^{o} of the c-axis. The existence of the strongly preferred growth direction in VSi_2, regardless of seed orientation is a direct consequence of the anisotropic crystal structure of VSi_2. Free energy considerations show that nucleation and subsequent growth in a direction perpendicular to the plane of closest packing of constituent atoms is strongly preferred, and in VSi_2 the basal planes are by far the densest-packed planes. This anisotrophy of growth must facilitate the growth of a single grain at the expense of peripheral grains of less favourable orientation, and explains the high success rate in single crystal growth of VSi_2 in the present work.

Having recorded a Laue photograph of the "as-grown" orientation, the procedure adopted was to tilt the crystal into the c-axis orientation using the goniometer, mount on the spark machine and cut a basal section and record a Laue photograph of the basal section. This provided a reference orientation from which the orientations required for the mechanical testing programme could be easily obtained.

Transmission electron microscopy specimens were prepared from the basal section cut from the as-grown crystal to assess the crystal perfection.

Fig. 3.5 Electron micrograph from as-grown crystal

Electron diffraction confirmed the single crystal nature of the crystals, and that low-angle grain boundaries only were present. Figure 3.5 shows a typical electron micrograph taken from an as-grown crystal. The main features of interest here are the dislocation density and the general distribution and nature of defects present. Immediately obvious is the low dislocation density. Dislocation density is defined as the length of dislocation line (in cms.) in 1 cm^3 of crystal. Assuming a specimen thickness of 3000Å the dislocation density estimated from Fig. 3.5 is 10^8cm, unexpectedly high for a melt-grown crystal suggesting some stressing of the sample. Other obvious features are the paired nature of dislocations present, and the lack of stacking fault ribbon contrast observed in as-grown crystals. These features will be discussed in detail below in discussion of plasticity of crystals.

REFERENCES

(1) Kieffer, R. and Benesovsky, F. Z. Metallk. 47, 247, (1956).

(2) Mayer, I. and Felner, I. J. Less Comm. Metals 37, 1763 (1974).

(3) Robins, D. A. and Jenkins, I. Acta Met. 3, 598, (1955).

(4) Goldschmidt, H. J. In: Interstitial Alloys; Butterworths, (1967) p.10.

(5) Hallais, J. Ann. Chim. (Paris) 6(5), 321, (1971).

(6) Kocherzhinskii, I. A., Kulik, V. and Shiskin, K., Dokl. Ak. Nauk S.S.R. 209 (6), 1347 (1973).

(7) Seeber, B. and Nickel, J. J. Phys. Stat. Sol (a) 15, 73, (1973).

CHAPTER 4

SINGLE CRYSTAL DEFORMATION

4.1 Plastic Anisotropy

When analysing compression test data on single crystals the applied stress must be resolved into shear stresses on the various possible slip systems. Only the resolved shear stress on the slip plane and in the direction of slip produces a glide force on a dislocation.

For an applied stress σ, the resolved shear stress τ on a given slip system, as shown in Fig. 4.1 is given by

$$\tau = \sigma \cos\varphi \cos\lambda \qquad 4.1$$

where the angles φ and λ are those between the normal to the glide plane and the compression axis and between the slip direction and the compression axis respectively. The expression $\cos\varphi\cos\lambda$ is known as the Schmid factor. To a very good approximation, slip always occurs first on the system on which the resolved shear stress is greatest, and slip is initiated when the critical resolved shear stress for that system is reached.

For a given compression axis the resolved shear stress on any system may be computed using 4.1. An alternative method which is particularly useful for crystals having non-cubic symmetry is to use a stereographic projection in conjunction with a plot of isostress contours as developed by Hartley and Hirth[1]. What is required is a stereographic projection

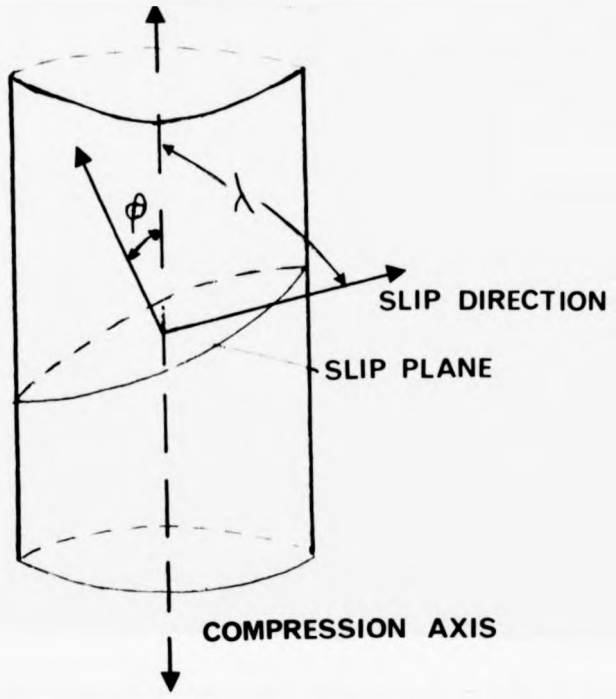

FIG. 4.1 Compression testing - Schmid factor

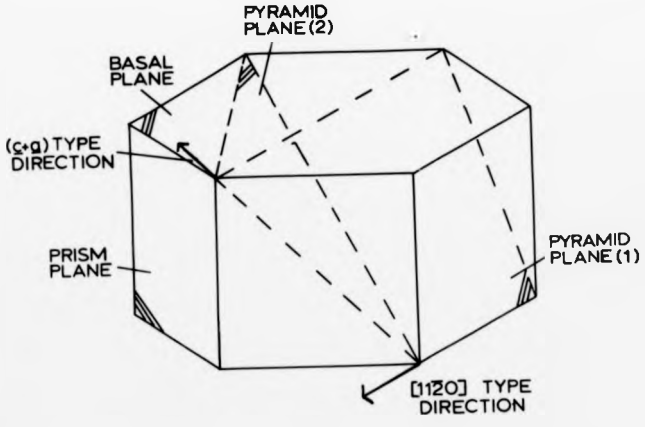

FIG. 4.2 Possible slip systems for hexagonal symmetry

along either the slip plane normal or the slip direction. The isostress map is superimposed on this, and the resolved shear stress on this system for any given compression axis is directly read off. This method will be discussed in detail below for basal slip in VSi_2.

Similar considerations apply to the measurements of strain obtained in a compression test. Here again the value of strain obtained must be expressed as a shear strain on the appropriate slip system. In this case the shear strain ε is given by

$$\varepsilon = \frac{\varepsilon_o}{\cos\varphi\cos\lambda} \qquad 4.2$$

where ε_o is the measured, i.e. longitudinal strain, and φ and λ are as defined in 4.1 above.

The choice of possible slip systems for any given crystal can be made on the basis of symmetry alone. Vanadium disilicide has hexagonal symmetry. Some possible slip systems for hexagonal symmetry are shown in Fig. 4.2. Slip planes usually correspond to rational low-index planes, particularly planes with weak atomic bonding and which have among the two or three largest interplanar spacings. The slip direction should, in general, correspond to one of the shortest perfect dislocation Burgers vectors. In hexagonal structures the basal plane (0001) is the favoured primary slip plane from the above considerations. This is certainly relevant to VSi_2, in which the bonding between basal planes is the comparatively weak Si-Si bond and the basal plane separation is the largest in the structure. The basal plane contains the a vector, the shortest

lattice translation vector of the type $\frac{a}{3}\langle\bar{1}120\rangle$, as do the prismatic $10\bar{1}0$ and pyramidal $10\bar{1}1$ planes. From symmetry alone then these are most probable slip systems in VSi_2.

4.2 Experimental Determination of C.R.S.S.

The single crystal deformation programme must provide quantitative information on the critical resolved shear stress (c.r.s.s.) for different possible slip systems. This was achieved by suitable choice of experimental compression axes as follows.

The first choice of compression axis was that for maximum resolved shear stress on the basal plane in the "close-packed" direction, i.e. on $\langle 11\bar{2}0\rangle$ (0001). This is illustrated in Fig. 4.3. This shows on stereographic projection along $\langle 0001\rangle$ for VSi_2. Below this is given a map of isostress contours. For maximum r.s.s. on $\langle 11\bar{2}0\rangle$ (0001), i.e. a Schmid factor of 0.5, the required compression axis is shown at A on the stereographic projection. Compression specimens of this orientation were cut after appropriate orientation of the as-grown crystal using the goniometer.

To obtain data on other slip systems, compression axes were selected for which the r.s.s. on these systems was much greater than on the basal system. To establish the operation of non-basal systems, compression axes were chosen for which there was zero r.s.s. on the basal system. The first axis chosen was B on Fig. 4.3, i.e. compression along $\langle 0001\rangle$, parallel to the c- axis. In this orientation, from 4.3, there is zero r.s.s. on the basal and any primatic system, so any pyramidal or other system will be activated.

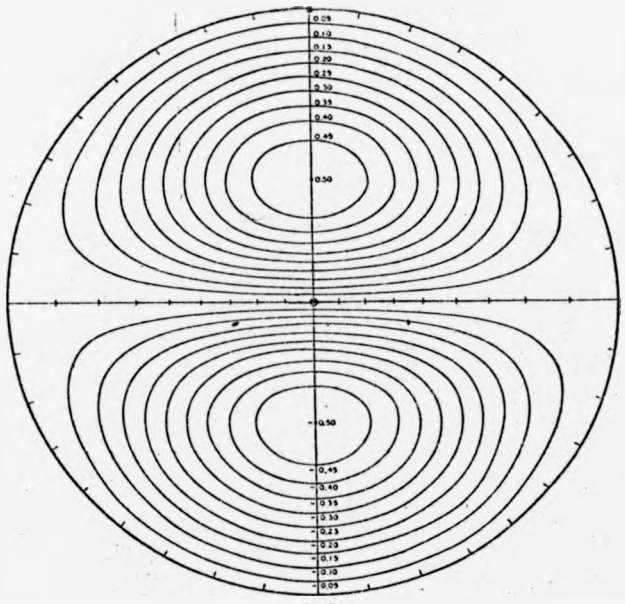

(a)

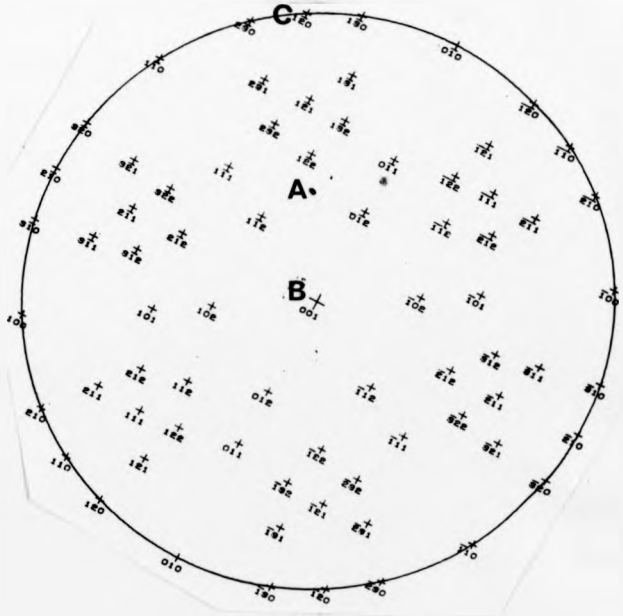

(b)

FIG. 4.3 Isostress contour technique for calculation of r.s.s. on given slip systems

(a) Isostress contour plot, after Hirth and Lothe[2]

(b) Projection on (0001) rotated for use in conjunction with (a), see p. 50.

Subsequent testing using compression axis C (Fig. 4.3), i.e. compression with the basal plane parallel to the compression axis will give a non-zero r.s.s. on prismatic and any other non-basal systems.

A compression testing programme carried out on crystals of these orientations enabled identification of the primary slip system and gave information on possible secondary systems. Quantitative information of the effects of orientation, temperature, composition and strain-rate on plasticity was obtained.

The data obtained from each test was in the form of a graph of total stress versus crosshead movement. To obtain a stress-strain curve from this data, both stress and strain were resolved into shear components acting along the appropriate plane and direction in that plane. Throughout the work described in this thesis it has been assumed that curves derived in this way are true stress-strain curves. The assumptions implicit in this are that (a) crystallographic axis rotation effects during compression may be neglected at the strains imposed, and (b) the stiffness of the compression apparatus is such that the elastic portion of the stress strain is characteristic of the specimen only. These assumptions are discussed in the Appendix to this Chapter, page 58.

A typical stress-strain curve is presented in Fig. 4.4 for $VSi_{1.80}$ basal slip, 800°C. In this work the flow stress has been taken as the stress at which the stress-strain curve departs from linearity, as shown in Fig. 4.4. The main feature of interest in the typical curve presented (Fig. 4.4) is the two-stage work-hardening observed. This is characteristic of plastic deformation of VSi_2 on the basal system.

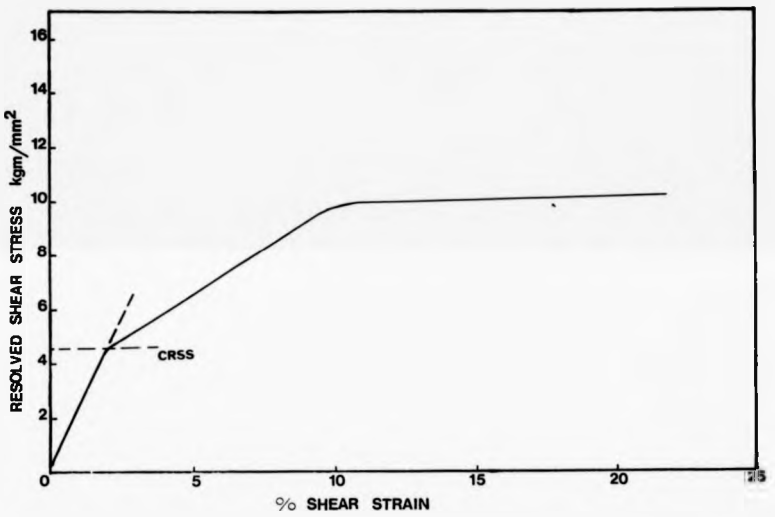

FIG. 4.4 Stress-strain curve. Basal slip in $VSi_{1.80}$ at 800°C

The results will be presented as successive sections on the dependence of flow stress on orientation, temperature and composition, followed by sections on strain-rate variation experiments and on work-hardening.

4.3 Effect of Orientation

The compression testing programme for determination of activated slip systems was carried out for each composition as described in 4.2 above.

The results obtained were similar for each composition; Table 4.1 shows a typical set of results obtained for $VSi_{1.70}$ at 1000°C. From these results, the stress for plasticity in specimens orientated for maximum r.s.s. on the basal system is an order of magnitude lower than for orientations with zero R.S.S. as the basal system. This means that in the temperature range studied the c.r.s.s. for the basal system is at least an order of magnitude less than for any other system at the same test temperature, i.e. the basal $\langle 11\bar{2}0\rangle$ (0001) system is the primary slip system operating in VSi_2.

4.4 Effect of Temperature

The first objective in the study of the temperature dependence of mechanical properties of VSi_2 was to establish the temperature at which plastic deformation was possible in specimens orientated for maximum r.s.s. on the primary system, i.e. a determination of the ductile to brittle transition temperature. Such a determination was carried out for each composition, and the transition temperature was found to be in the range 650-750°C for all compositions. This is a

Compression Axis orientation to c- axis	Flow Stress kgm/mm^2
45^{o}	3
parallel	>30
perpendicular	>30

TABLE 4.1 Orientation dependence of flow stress $VSi_{1.70}$ at $1000^{o}C$

homologous temperature in the range 0.55-0.62 T_m where T_m is the melting point of VSi_2. This is typical of inherently strong solids which have brittle to ductile transition temperatures of 0.4-0.6 T_m.

Data on the variation of flow stress with temperature is essential for an assessment of vanadium disilicide as an engineering material, and for a discussion of deformation mechanisms operating in VSi_2. For each composition the variation of c.r.s.s. with temperature in the range 700 to 1200°C was determined for the basal, primary, slip system and for compression along <0001> (c-axis) and <1120> (perpendicular to c-axis).

Figure 4.5 shows the temperature dependence of c.r.s.s. for basal slip for various compositions. The main feature here is the decrease in flow stress with temperature.

The results on the other orientations are much less well-defined. Specimens compressed parallel to the c-axis and along $\langle 11\bar{2}0 \rangle$ did not deform plastically below 1000°C, and failed by longitudinal brittle fracture. At temperatures above 1000°C deviations from linearity in the stress-strain curves were observed at high stresses, e.g. in $VSi_{1.80}$ compressed along <0001> such deviations were observed at loads of 550 kgm. at 1000°C and 200 kgm. at 1200°C, and for compression along $\langle 11\bar{2}0 \rangle$ deviation was observed at a load of 700 kgm. at 1000°C. The evidence here suggests thermal activation of a secondary possibly pyramidal slip system which could become important at elevated temperatures. Even at 1200°C, a load of 200 kgm. is equivalent to a flow stress of approximately 10 kgm/mm^2

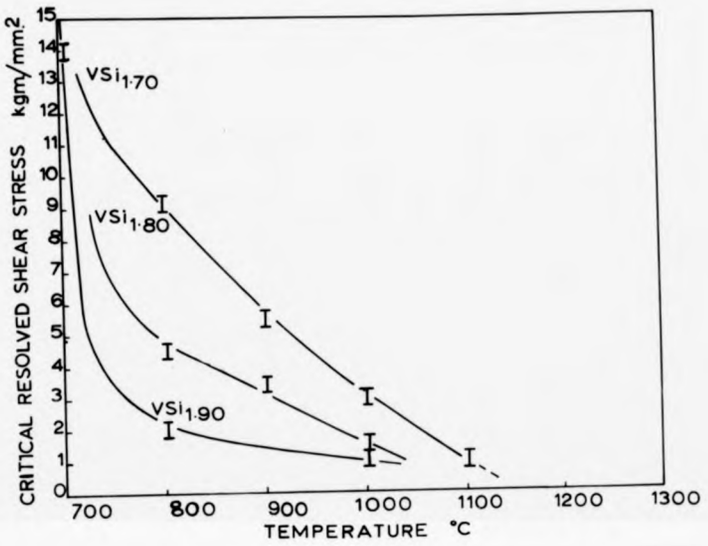

FIG. 4.5 C.R.S.S. versus temperature curves

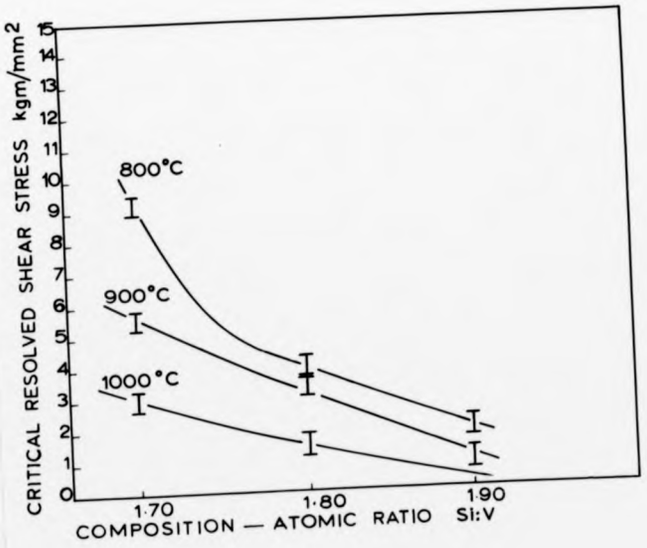

FIG. 4.6 C.R.S.S. versus composition curves

assuming a pyramidal system, i.e. a flow stress on order of magnitude higher than for basal slip. The possibility of a secondary system or the accommodation of plastic strain at these high stress levels by basal slip due to mis-orientation of the specimen will be dealt with later.

The high temperature testing programme also gave information on the oxidation properties of VSi_2. All testing was done in air, and at temperatures of up to 1000°C there was little or no change in the specimen from the as-prepared condition. There were signs of preferential formation of an oxide layer in islands on the surface in some cases. At 1200°C the oxide layer had completely formed, giving the specimen a bluish colour. There was no catastrophic oxidation such as to cause anything other than surface effects. The oxidation behaviour will be discussed in detail in Chapter 5 below. The point of relevance here is that the mechanical properties may be justifiably assumed to be independent of oxidation effects in the temperature range studied.

4.5 Effect of Composition

A set of curves of flow stress versus crystal composition for basal slip at various temperatures is given in Fig. 4.6. This figure shows the marked reduction in c.r.s.s. towards the stoichiometric composition at all temperatures which is rather a surprising result. This composition effect is much less marked at higher temperatures, indicating the possibility of a diffusion effect becoming significant. These results are important in connection with the discussion in Chapter 6 below on deformation mechanisms.

The effect of composition of specimens compressed with zero r.s.s. on the primary system was also studied. As in the case of temperature dependence above, the results for these orientations are less well defined. The substance of the results is that with increasing deviation from stoichiometry lower stresses are required for plasticity or fracture for specimens of the same orientation at the same temperature. For example, for <0001> compression at 1000°C the total loads at which there was evidence for plasticity were for $VSi_{1.90}$, $VSi_{1.80}$ and $VSi_{1.70}$, 650, 550 and 325 kgm. respectively, these results obtained under identical conditions. In this case the effect of composition is the opposite to that for basal slip, indicating that a different mechanism is operating. These results again are consistent with the high temperature activation of a secondary slip system.

4.6 Effect of Strain Rate

All the compression testing reported above was performed at a strain rate of 0.005 cm/min. to ensure the validity of direct comparison of results. However, it is also of interest to study the strain rate dependence of flow stress. Performing differential strain rate tests is an established technique for the determination of the activation volume which may assist in identification of the rate-controlling deformation mechanism[1]. In this type of test compression is commenced at a constant strain rate in the usual way, then the strain rate is given regular increments and the load increase noted.

Figure 4.7 shows such a test for $VSi_{1.70}$, orientated for basal slip at 1000°C. The strain rates used were successively 0.002, 0.005, 0.01 and 0.02 cm/min.

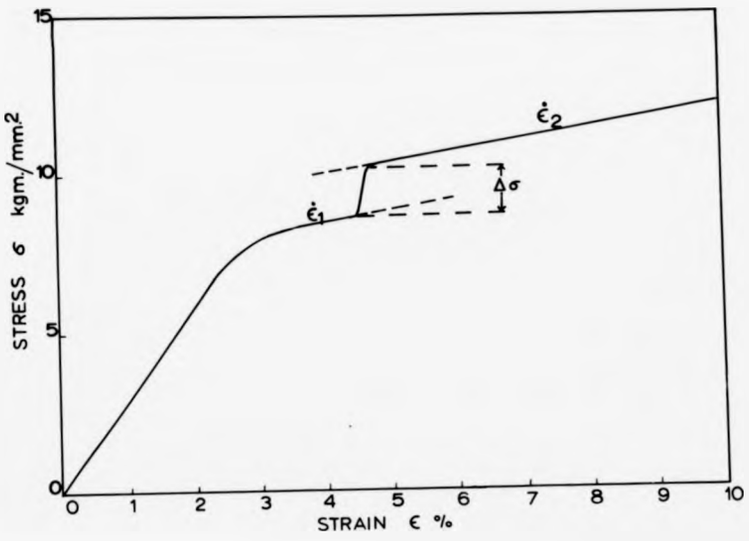

FIG. 4.7 Strain rate dependence results, $VSi_{1.70}$, 1000°C.
$\dot{\epsilon}_1 = 0.002\ cm.\ min^{-1}$; $\dot{\epsilon}_2 = 0.005\ cm\ min^{-1}$.

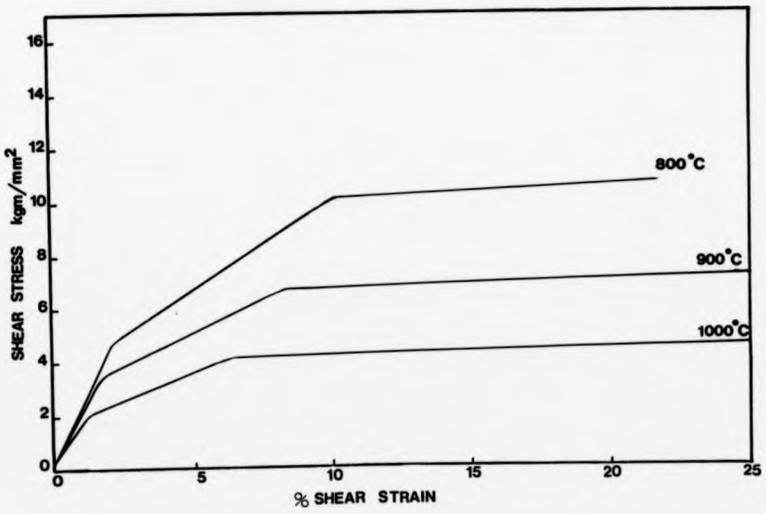

FIG. 4.8 Family of stress-strain curves for $VSi_{1.80}$

The activation volume $V^{\times}$ is defined as follows. When a segment of dislocation, of length l and Burgers vector b, moves from its equilibrium position to overcome an obstacle, the minimum Gibb's free energy required is

$$\Delta G = \Delta g - \tau^* \; l \; b \Delta R \quad - 4.3$$

where Δg is the change in free energy of localised atomic displacements during activation, τ^* is the effective stress and ΔR is the activation distance.

The application of this equation is restricted to reversible, isothermal processes. Most thermally activated deformation processes are considered to satisfy this requirement.

Then $V^* = l \; b \Delta R$ is the activation volume.

For dislocations of one type, the strain rate $\dot{\epsilon}$ is given by the Arrhenius type rate equation

$$\dot{\epsilon} = \dot{\epsilon}_o \exp \left(-\frac{\Delta G}{kT}\right) \quad - 4.4$$

By differentiating 4.3 with respect to effective stress,

$$\left(\frac{\partial \Delta G}{\partial \tau^*}\right)_T = - V^* \quad - 4.5$$

and using 4.4

$$V^* = kT \left(\frac{\partial \ln \frac{\dot{\epsilon}}{\dot{\epsilon}_o}}{\partial \tau^*}\right)_T = kT \left(\frac{\partial \ln \dot{\epsilon}}{\partial \sigma}\right)_T \frac{1}{\cos\varphi\cos\lambda} \quad - 4.6$$

where $\cos\varphi\cos\lambda$ is the Schmid factor $= \frac{1}{2}$ for c.r.s.s. max as in the test described here.

Then for small values of $\Delta\sigma$,

$$V^* \simeq 2kT \left(\frac{\Delta \ln \dot{\epsilon}}{\Delta \sigma}\right) \quad - 4.7$$

The value for the activation volume V^* from 4.7 for the test of Fig. 4.7 is approximately $20b^3$ where b is the magnitude of the Burgers vector $\frac{a}{3}\langle 11\bar{2}0\rangle$. Discussion of the use of this

value of V^* in determining deformation mechanisms is given in Chapter 6 below. The activation volume could be determined for basal slip only because of the high stress levels involved in the possible secondary slip described above.

4.7 Work-Hardening Observations

From Fig. 4.4, which is a typical stress-strain curve obtained for basal slip, a two-stage work-hardening was observed in which at the onset of plasticity there is a region of high work-hardening followed by a stage of almost zero work hardening. The features of interest here are the strains at which these stages of hardening occur, an estimate of the magnitude of the hardening in the two stages, and the effect of composition and temperature on the work-hardening behaviour.

Typical values of shear strain observed in the three stages of deformation were 2% elastic, 8% stage I and 10% stage II. Figure 4.8 shows a family of stress-strain curves obtained for $VSi_{1.80}$ at a range of temperatures. The work-hardening rates in stages I and II are similar in all cases, the effect of increasing temperature is to lower the amount of stage I (high) work-hardening. A similar effect was observed for each composition.

Figure 4.9 shows a set of stress-strain curves for basal slip at 800°C for various compositions. The effect here is very small; if anything, deviation from stoichiometry has the same effect as increasing temperature, i.e. a reduction in stage I hardening.

value of V^* in determining deformation mechanisms is given in Chapter 6 below. The activation volume could be determined for basal slip only because of the high stress levels involved in the possible secondary slip described above.

4.7 Work-Hardening Observations

From Fig. 4.4, which is a typical stress-strain curve obtained for basal slip, a two-stage work-hardening was observed in which at the onset of plasticity there is a region of high work-hardening followed by a stage of almost zero work hardening. The features of interest here are the strains at which these stages of hardening occur, an estimate of the magnitude of the hardening in the two stages, and the effect of composition and temperature on the work-hardening behaviour.

Typical values of shear strain observed in the three stages of deformation were 2% elastic, 8% stage I and 10% stage II. Figure 4.8 shows a family of stress-strain curves obtained for $VSi_{1.80}$ at a range of temperatures. The work-hardening rates in stages I and II are similar in all cases, the effect of increasing temperature is to lower the amount of stage I (high) work-hardening. A similar effect was observed for each composition.

Figure 4.9 shows a set of stress-strain curves for basal slip at 800°C for various compositions. The effect here is very small; if anything, deviation from stoichiometry has the same effect as increasing temperature, i.e. a reduction in stage I hardening.

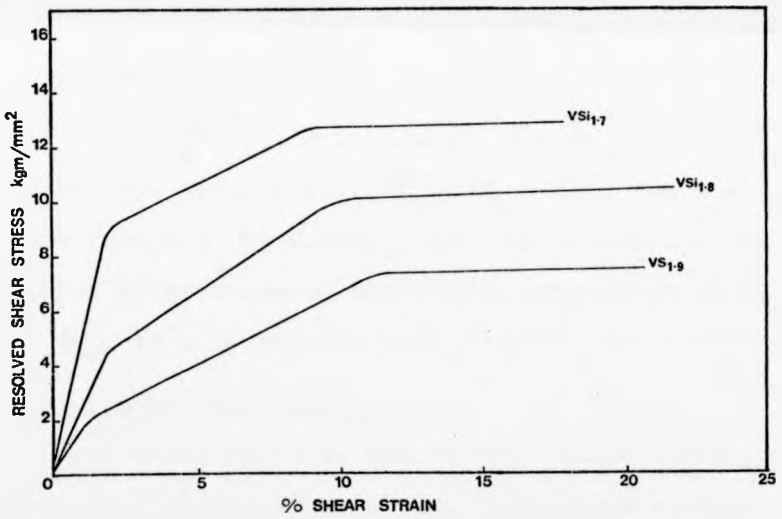

FIG. 4.9 Family of stress-strain curves, 800°C

Appendix

(a) Lattice Rotation During Compression

In the case of compression of a crystal between flat plates, as in the present work, the normal to the slip plane approaches the compression axis by rotation about an axis parallel to the line of intersection of the slip plane and the compression plates.

If the initial height of the specimen is h_o and the height after compression is h, after a shear strain α, then

$$\frac{h_o}{h} = \frac{\sin \varphi_o}{\sin \varphi} \qquad 4.8$$

where φ_o and φ and λ_o and λ are the initial and final values of the angles φ and λ as defined in Fig. 4.1.

It can be shown that

$$\left(\frac{h_o}{h}\right)^2 = 1 + 2\alpha \cos \varphi_o \cos \lambda_o + \alpha^2 \cos^2 \lambda_o. \qquad 4.9$$

For the present work, $\varphi_o = \lambda_o = 45^o$, for a shear strain of 10% from 4.9 $h = 0.95\, h_o$, and the assumption that lattice rotation affects may be neglected, equivalent to assuming $h = h_o$, is a reasonable one.

(b) Stiffness of Apparatus

From examination of the stress-strain curves, e.g. Fig. 4.4 the elastic region shows a very low apparent elastic modulus for VSi_{2-x}. This shows that the assumption of a high stiffness of the compression apparatus is not valid, and this should be borne in mind when studying the stress-strain curves. Determination of C.R.S.S. and analysis of work-hardening based on the given curves is unaffected.

References

(1) Evans, A. G. and Rawlings, R. D. Phys. Stat. Sol. 34, 9, (1969).

(2) Hirth, J. P. and Lothe J. In "Theory of Dislocations" McGraw-Hill, New York (1968).

CHAPTER 5

MICROSTRUCTURAL ANALYSIS OF DEFORMED CRYSTALS

5.1 Optical Metallography

5.1.1 Slip Trace Analysis

Two surface analysis enables the slip plane to be indexed if the angles of intersection of the slip plane, as measured by the slip traces, with two known planes can be obtained.

Figure 5.1 illustrates the procedure used.

Figure 5.1(a) represents the deformed crystal. For convenience a rectangular specimen is used. The slip plane cuts the perpendicular faces A and B in directions $\underline{P}_A$ and $\underline{P}_B$ respectively, i.e. the slip lines are observed optically in these directions, making angles α and β with the edge of the crystal.

The poles of faces A and B are known from Laue photographs. Stereographic projection is used to analyse the results, as in Fig. 5.1(b). The poles of A and B are plotted on a stereogram and the edge direction $\underline{E}$ is given by the intersection of the great circles corresponding to these poles. $\underline{P}_A$ and $\underline{P}_B$ are plotted by measuring α and β degrees respectively from $\underline{E}$ along the great circles A and B. The slip plane P is then given by the pole of the great circle joining $\underline{P}_A$ and $\underline{P}_B$, and may readily be indexed.

Provided slip lines can be unambiguously observed on perpendicular faces of the deformed crystal, indexing of the slip plane by the above technique is straightforward. The determination of the slip direction is not so easily achieved.

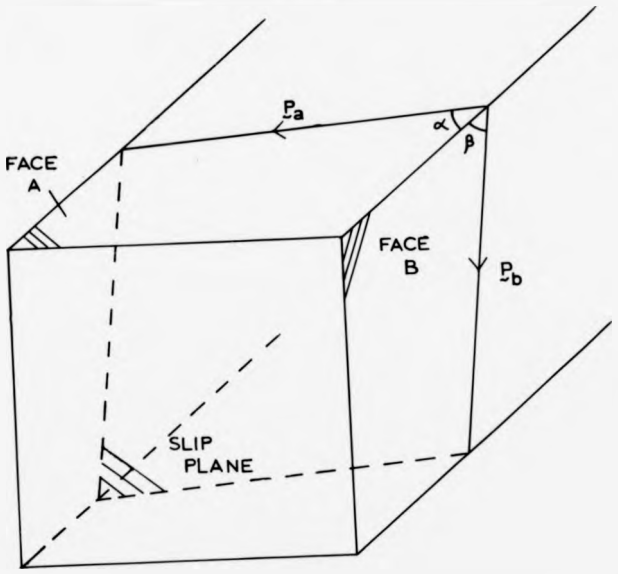

FIG. 5.1(a) Slip lines on crystal faces

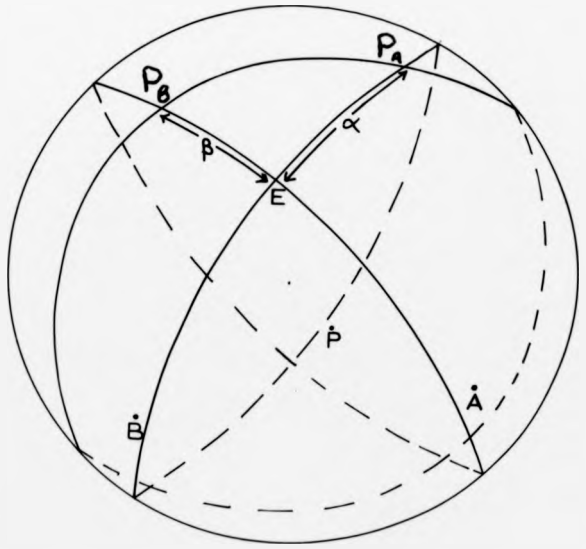

FIG. 5.1(b) Stereographic representation

This must be done by observing the direction in the slip plane in which the slip steps are a minimum, or, ideally, zero. The slip direction is then at right angles to this direction. Rectangular specimens are inconvenient for this procedure, because two surfaces only may be studied, and in practice confirmation of the slip direction by transmission electron microscopy, as described in 5.2 below, is the most reliable technique.

The deformed vanadium disilicide crystals, tested as described previously, were amenable to two-surface analysis for test temperatures below about 1000°C. At higher temperatures, surface oxidation made the optical observation of slip lines very difficult.

For slip-plane determination, optical micrographs of adjacent perpendicular faces were recorded. Figure 5.2 shows the slip lines observed on a typical crystal, oriented for easy basal (0001) slip, and Fig. 5.3 shows the stereographic projection analysis which confirms that (0001) is the operative slip plane.

This analysis was performed on each deformed crystal, and (0001) confirmed as the primary slip plane.

For crystals oriented for zero resolved shear stress on the basal system, the analysis was complicated by the fact that temperatures above 1000°C, and higher stress levels were required for plasticity. Slip lines were not readily visible on optical examination, and in most cases macroscopic shape changes were the only indication of slip in the absence of direct electron microscopic observation. In some c-axis

FIG. 5.2 Basal slip at 800°C Mag. x500

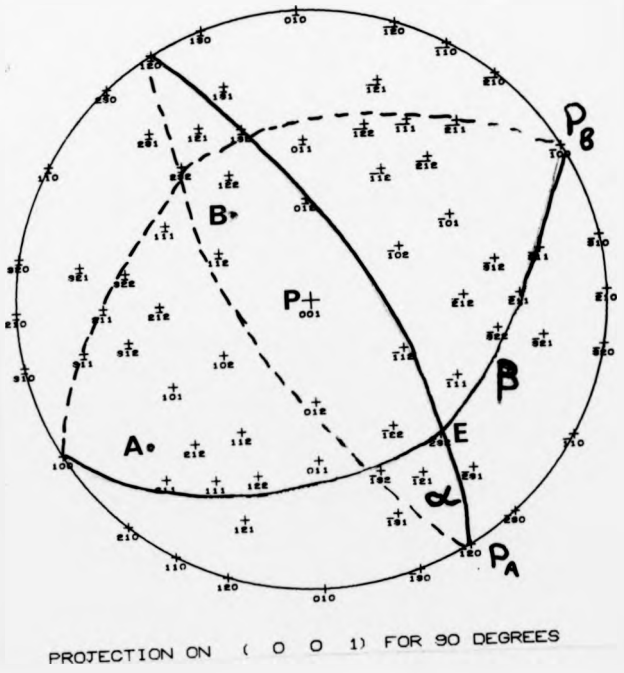

FIG. 5.3 Stereographic projection

compression specimens which had deformed plastically there were visible slip lines which indicated that in these cases also, basal slip was operative. The possibility of basal slip in c-axis compression will be discussed in Chapter 6.

In no specimens were non-basal slip lines observed, and the indication from optical work is therefore that basal slip is the only active slip plane at temperatures below 1200°C.

The crystals which were oriented for easy basal slip had maximum resolved shear stress in a close-packed direction that is the Schmid factor = $\frac{1}{2}$, $\lambda = \varphi = 45^{\circ}$ (see Fig. 4.1).

The faces of the compression specimen were then cut parallel and perpendicular to this direction to confirm by the magnitude of the slip-steps that this was in fact the slip-direction. The results obtained in this way were inconclusive. In some specimens the maximum offset was observed perpendicular to the expected slip direction, but in no case was a zero offset observed on the face parallel to that direction, possibly because of the relatively large amounts of plastic strain, usually about 10%, applied.

5.1.2 Macroscopic Features

The macroscopic features of each deformed crystal were recorded by taking low-magnification (8x) photographs of two perpendicular faces of the compression specimen. An example is given in Fig. 5.4 for easy basal slip.

An indication of the slip direction can usually be obtained from the geometry of the deformed specimen, and this coupled with the measurement of slip steps was in many cases

Fig. 5.4 Macroscopic deformed crystal. Perpendicular faces. Basal slip at 800°C

sufficient to confirm a slip direction of the type $\{11\bar{2}0\}$, the close-packed direction, as expected from consideration of possible Burgers vectors.

These low magnification photographs illustrate the marked anisotropy in the deformation behaviour of VSi_{2-x} under compression.

At high plastic strains, specimens oriented for basal slip fail by propagation of longitudinal cracks initiated by constriction of the ends of the specimen during the test.

5.1.3 Oxidation Behaviour

Optical microscopy was the most useful technique for characterising the oxidation behaviour of vanadium disilicide.

At test temperatures below 800°C, oxidation was minimal and the samples retained their as-polished finish. Initial stages of oxidation were observed to occur in isolated patches.

In the temperature range from 900°C upwards, oxidation progressed until at 1200°C a complete bluish skin had formed over the sample. At no time was anything more than surface oxidation observed. Figure 5.5 shows the progressive oxidation in the range 800-1200°C.

The formation of self-healing protective layers in silicides at elevated temperatures has been known for some time and as outlined in Chapter 1 is one of the features which make silicides potential high temperature materials.

In the course of work[1] on $MoSi_2$ as furnace elements, the formation of a protective layer stable up to 1800°C was observed and the survey by Kieffer and Benesovsky[2] reported maximum oxidation resistance in several metal-silicon systems

(a)

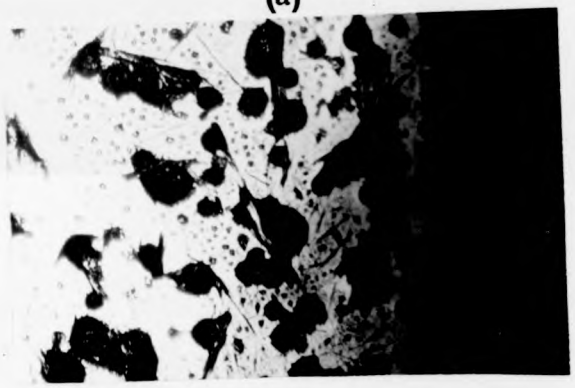

×200

(b)

(c)

FIG. 5.5 Oxidation Behaviour

(a) 800°C
(b) 1000°C
(c) 1200°C

at the disilicide composition. The phenomenon of low temperature disintegration ("pest" effect) has been observed in $MoSi_2$[3] and in other disilicides[4], W, Cb and Fe. In this effect disintegration of the sample occurs over a finite temperature range, usually in the range 500-1000°C, in the presence of a reactive gas, e.g. oxygen. The effect has been observed in single crystals, but it is smaller than in polycrystalline materials, suggesting a grain boundary effect.

The work of Schwettman et al.[5] on the oxidation behaviour of $TiSi_2$ is of particular relevance to the present work. They report the formation of an amorphous surface film at 600°C and propose the reaction

$$6TiSi_2 + 10O_2 = TiO_2 + 9SiO_2 + Ti_5Si_3 \quad — 5.1$$

with the formation of a silicate glass on the surface. At 800°C a significant change in the structure of the film was observed. Small islands of crystalline material were observed on top of the amorphous layer which were identified as TiO_2 in the rutile form. As oxidation time increased, more islands were formed, and the original islands grew in size.

At higher temperatures, 1200°C, the main difference was the detection of α-cristobalite by X-ray methods, and crystalline islands of α-cristobalite were observed optically after longer oxidation times (30 hrs).

These observations agree well with the present observations on VSi_2, and a similar mechanism is almost certainly operating. Recent Russian[6] work on oxidation of polycrystalline VSi_2 confirms the presence of V_5Si_3 after oxidation.

The "pest" phenomenon has been attributed to the formation of oxides at temperatures below the critical for formation of the glassy phase, e.g. MoO_3, and their subsequent volatilisation. Since TiO_2 is the highest oxide of titanium and is not volatile at any temperature studied, it is probable that the "pest" effect will not be observed in $TiSi_2$. In the case of VSi_2, there is a higher, comparatively volatile oxide V_2O_5 which could lead to disintegration low temperatures. This effect has not been observed in the current work, even in lengthy anneals at temperatures as low as 400°C.

Another possibility explanation of the non-occurrence of the "pest" effect in $TiSi_2$ and possibly in VSi_2 is that the protective glassy layer can form at low temperatures.

TiO_2 is partially soluble in SiO_2 [7], hence a titania-silica glass may form readily. No phase diagram data on the V-O-Si system is available, but a similar affect may well occur.

5.2 Electron Microscopy

5.2.1 Introduction

Accelerated electrons incident on a sufficiently thin crystal in a parallel mono-chromatic beam are not only transmitted without change in direction, but emerge also in a number of different discrete directions.

The wave vectors $\underline{k}$ and $\underline{k}_o$ of scattered and incident beam satisfy the Bragg law

$$\underline{k} - \underline{k}_o = \underline{g} \qquad 5.2$$

where $\underline{g}$ is a reciprocal lattice vector.

For elastic scattering $k_o = /\underline{k}_o/ = /\underline{k}/ = \frac{1}{\lambda}$, where λ is the wavelength of the incident electrons.

The Bragg law may be expressed as

$$\sin\theta_B = \frac{g}{2k_o} = \frac{n\lambda}{2d_{hkl}} \quad -5.3$$

where $2\theta_B$ is the angle between $\underline{k}$ and k_o, n is an integer, and d_{hkl} is the inter-planar spacing of the reflecting planes. For 200 KeV electrons $\lambda = 0.025\text{Å}$, and d_{hkl} is $\sim 3\text{Å}$, hence θ_B is very small, and the incident beam is almost parallel to the diffracting crystal planes.

Most of the electron microscopy described in this thesis has been performed using the "two-beam" condition, in which the sample is tilted such that only one strong diffracted beam is operating. The theory for this special case is well developed, and contrast features and defect analysis may be explained in terms of this two-beam theory.

The intensity of the diffracted beam is given by[8]

$$|\varphi_g|^2 = \left(\frac{\pi^2}{\xi_g}\right)^2 \frac{\sin^2(\pi t s_{eff})}{(\pi s_{eff})^2} \quad -5.4$$

Where t is the sample thickness, ξ_g is the extinction distance, i.e. the sample thickness at which the diffracted beam has been completely re-diffracted into the incident direction. S_{eff} is a parameter defining the deviation from the exact Bragg condition.

Equation 5.4 shows the means by which contrast may arise in electron microscopy.

Variation in specimen thickness produces contrast, but the most important feature in the present work is contrast from variation in S_{eff}. Crystal imperfections such as dislocations may be considered as local variations in crystal orientation which is equivalent to a local variation in S_{eff}.

Since the Bragg angle is very small for low-order reflections, even small crystal distortions will not be small compared to the Bragg angle, and contrast will result.

The use of contrast experiments in the electron microscope to determine the Burgers vector of a dislocation is a well-established technique. The specimen is tilted into a strong two-beam condition in which the dislocation of Burgers vector $\underline{b}$ is in poor contrast. For elastically isotropic materials, the dislocation image becomes invisible when $\underline{g} \cdot \underline{b} = 0$. For pure screw dislocations this is a sufficient condition for invisibility. For a pure edge or for a mixed dislocation of line vector $\underline{u}$ the additional condition $\underline{g} \cdot \underline{b} \times \underline{u} = 0$ must be satisfied. This latter term may usually be minimised so that for $\underline{g} \cdot \underline{b} = 0$ the dislocation is effectively invisible. This is usually the case for $\underline{g} \cdot \underline{b} \times \underline{u} \leq 0.64$. To identify $\underline{b}$ unambiguously the invisibility criterion must be satisfied for two or more different diffracting vectors $\underline{g}$. The determination of the sign of $\underline{b}$ may also be determined provided the signs of Seff and $\underline{g}$ are known. Under some conditions very strong images can be obtained when $\underline{g} \cdot \underline{b} = 0$ and $\underline{g} \cdot \underline{b} \times \underline{u} \leq 0.64$ due to elastic anisotropy of the material for $g = \langle 0003 \rangle$ (see Fig. 5.6).

5.2.2 Experimental Observations of Basal Dislocations

Specimens for electron microscopy were prepared as described in Chapter 2. Most of the sections were cut parallel to the basal plane, which had been established as the primary slip plane, to obtain maximum dislocation density in the electron transparent region.

The dislocation arrangements shown in Fig. 5.6 are typical of those observed in deformed material. The characteristic feature is the occurrence of dislocations in pairs. The possible situations in which a double dislocation may occur are as follows:- (a) the dissociation of a perfect dislocation into partials, (b) the interaction of two perfect dislocations of opposite sign to form a dislocation dipole, (c) the interaction of two dislocations of the same sign to form a "superlattice" dislocation as observed in ordered alloys. In addition, there are two situations in which a double image of a single dislocation may occur (a) when a second reflection is weakly excited in a nominally two beam situation in bright field and (b) when $\underline{g} \cdot \underline{b} = 2$. It should be straightforward to distinguish these "spurious" cases from pairing of dislocations.

The analysis in the present case will be discussed with reference to Fig. 5.7, an (0001) projection of the atomic arrangement in VSi_2. On this projection are shown the unit cell, and possible dislocation dissociations in the B layer of the structure. The perfect slip dislocation has the lattice translation vector of the type $\frac{a}{3}$ $\langle 11\bar{2}0\rangle$, i.e. $\underline{a}$ in Fig. 5.7. The only possible dissociation of this perfect dislocation is into two half-partials, each with Burgers vector $\frac{a}{6}\langle 11\bar{2}0\rangle$ bounding a stacking fault, e.g. $\underline{b}_1$ and $\underline{b}_1^1$ in Fig. 5.7. It is important to realise that the three possible dissociations of this type within the same layer are not equivalent. Considering the three possible half partial translations $\underline{b}_1$, $\underline{b}_2$ and $\underline{b}_3$, the changes in stacking sequence are shown in Fig. 5.8, in which changes in the perfect

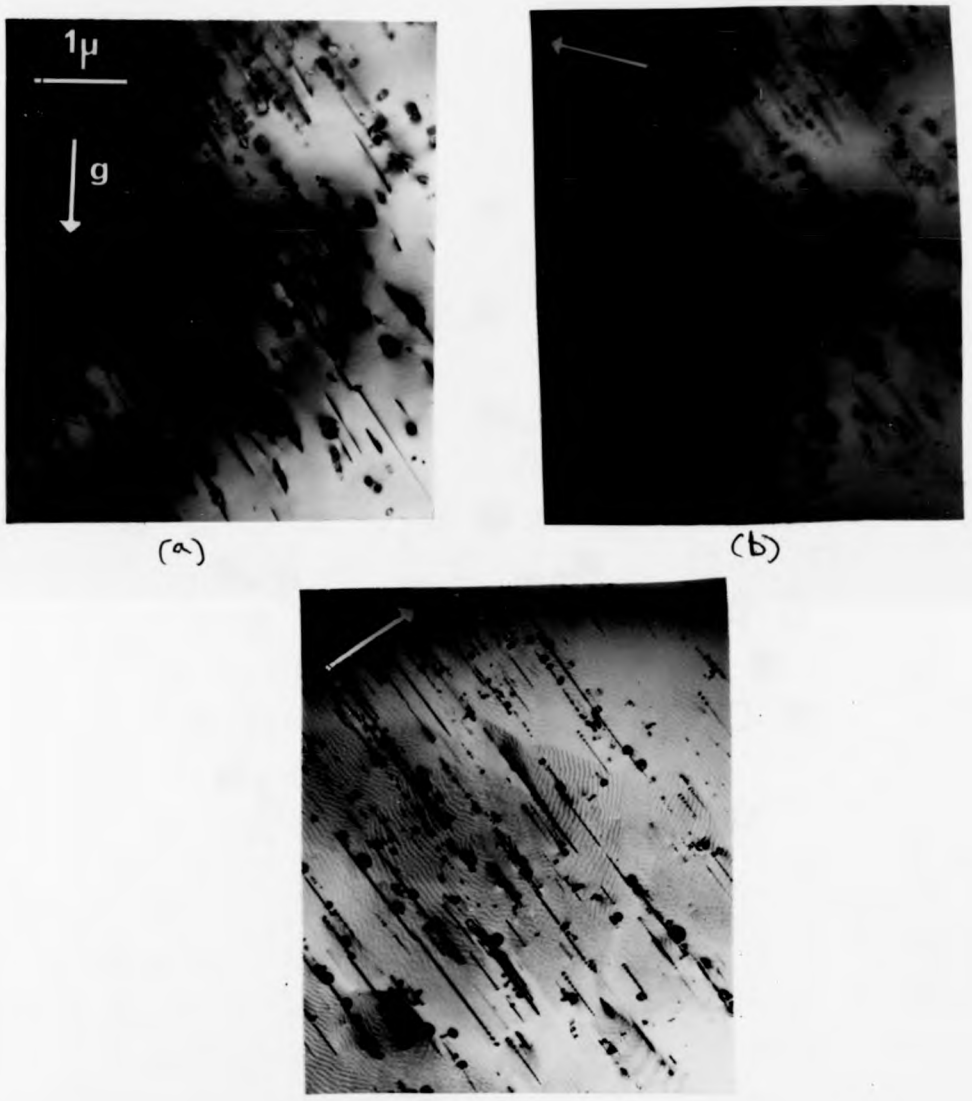

FIG. 5.6 Dislocation arrangement in deformed crystal.

(a) $\underline{g}$ = $\langle 11\bar{2}0 \rangle$
(b) $\underline{g}$ = $\langle 10\bar{1}1 \rangle$
(c) $\underline{g}$ = $\langle 0003 \rangle$

PLANE OF SAMPLE IS 15½° OFF (0001)

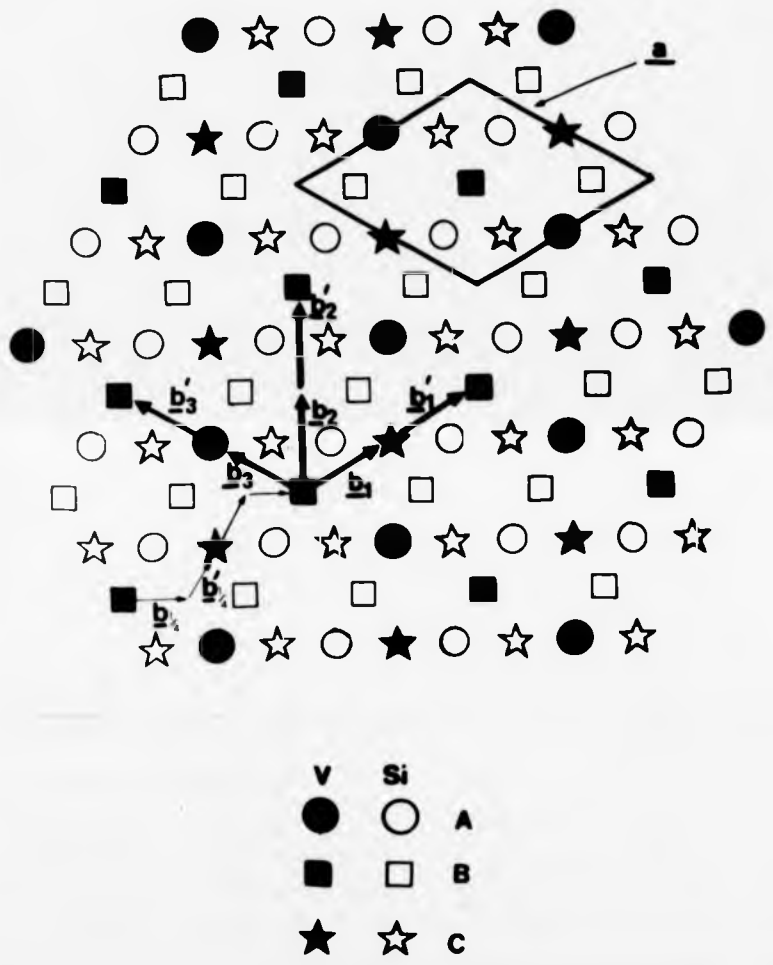

FIG. 5.7 (0001) projection showing possible dislocation dissociations.

ABCABCA... stacking are shown for each possibility. The positions A^1, B^1 and C^1 are equivalent, and are the sites left vacant in the perfect structure. $\underline{b}_2$ Is energetically the most favourable translation, because here the nearest neighbour distances are left unchanged after translation into the normally unoccupied sites. $\underline{b}_1$ Is the next most possible, and $\underline{b}_3$ least because in that case two identical layers would be superimposed. It seems from nearest neighbour considerations that the dissociation of a perfect slip dislocation into two half partials with the formation of a stacking fault with fault vector $\underline{R}_{\frac{1}{2}} = \frac{a}{6}\langle 11\bar{2}0\rangle$ is energetically favourable. A further dissociation of each half-partial into quarter partials $\underline{b}1/4$ with Burgers vector of the type $\frac{a}{6}\langle 10\bar{1}0\rangle$ is possible, and is shown in Fig. 5.7. In this case there is a considerable change in nearest neighbour co-ordination for a translation of the $\underline{b}1/4$ type, and the dissociation into quarter partials is less likely than the half-partial situation described above. Figure 5.9 shows a diagrammatic summary of the possible dissociation of the perfect dislocation $\underline{b}$ into quarter partials. The different energies involved are reflected in the greater width of dissociation of the half-partials compared to the quarter partials. Dissociation widths are estimated to be of the order of 80Å for half-partials and 20Å for quarter partials, see Appendix, page 73.

Experimental observation as shown in Fig. 5.6 did not reveal any stacking fault fringe contrast between widely separated partials as predicted above. Table 5.1 shows a calculation of $\underline{g} \cdot \underline{b}$ products for extinction conditions for

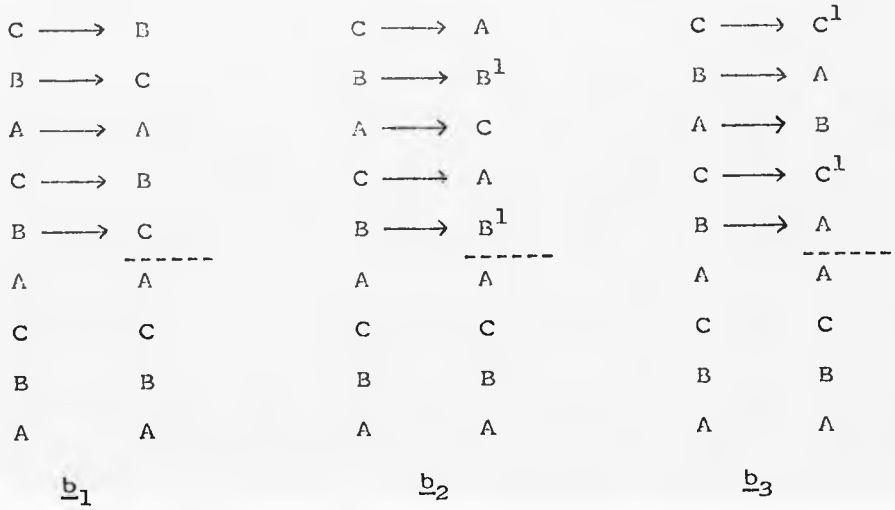

FIG. 5.8 Possible stacking faults

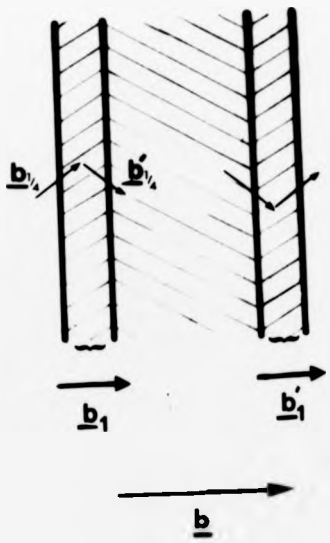

FIG. 5.9 Dissociation of slip dislocation into quarter partials

$\underline{b} = \frac{a}{3}\langle 11\bar{2}0\rangle$; $R\frac{1}{2} = \underline{b}\frac{1}{2} = \frac{a}{6}\langle 11\bar{2}0\rangle$; $R\frac{1}{4} = \frac{a}{6}\langle 10\bar{1}0\rangle$

$\underline{g}$	$\underline{g} \cdot \underline{b}$	$\underline{g} \cdot \underline{b}\frac{1}{2}$	$\underline{g} \cdot \underline{b}\frac{1}{4}$	$\alpha\frac{1}{2}$	$\alpha\frac{1}{4}$
$\langle 0003\rangle$	0	0	0	0	0
$\langle 10\bar{1}0\rangle$	a	$\frac{1}{2}$a	$\frac{1}{3}$ a	$\bar{1}\bar{1}$	$\frac{2}{3}\bar{1}\bar{1}$
$\langle 01\bar{1}0\rangle$	a	$\frac{1}{2}$a	$\frac{1}{6}$ a	$\bar{1}\bar{1}$	$\frac{1}{3}\bar{1}\bar{1}$
$\langle 1\bar{1}00\rangle$	0	0	$\frac{1}{6}$ a	0	$\frac{1}{3}\bar{1}\bar{1}$
$\langle \bar{1}120\rangle$	2a	a	$\frac{1}{2}$ a	$2\bar{1}\bar{1}$	$\bar{1}\bar{1}$
$\langle 2\bar{1}\bar{1}0\rangle$	a	$\frac{1}{2}$a	$\frac{1}{2}$ a	$\bar{1}\bar{1}$	$\bar{1}\bar{1}$
$\langle \bar{1}2\bar{1}0\rangle$	-a	$-\frac{1}{2}$a	0	$-\bar{1}\bar{1}$	0

TABLE 5.1 Extinction criteria

all the Burgers vectors discussed above, and phase angles $\alpha = 2\pi \underline{g} \cdot \underline{R}$ for stacking fault visibility for $\underline{R}_{\frac{1}{2}}$ and $R1_{/4}$. Using these criteria, the lack of contrast for $\underline{g} = \langle 10\bar{1}1 \rangle$ and $\langle 0003 \rangle$ showed that the Burgers vectors of the observed dislocations were indeed of the $\langle 11\bar{2}0 \rangle$ type, but were undissociated. The "dotted" contrast observed for $g = \langle 0003 \rangle$ is characteristic of basal dislocations in hexagonal close packed metals, although in the present work this residual contrast is relatively strong.

Dislocations may exist in pairs of like or unlike Burgers vectors. Like pairs are termed superlattice dislocations in alloys in which ordering occurs, but the term is not applicable here as VSi_2 is fully ordered up to its melting point. Unlike pairs are dislocation dipoles. The problem of distinguishing between the above cases has been given some attention in the literature[12, 13, 14].

The properties of a dipole (unlike Burgers vectors) which can be used to distinguish it from a pair of like sign are as follows:-

(a) The spacing between dipole components changes if reflections +g and -g for the same sign of S, or +S and -S for same sign of g, are used[12].

(b) The image of a dipole possesses a centre of inversion if the dipole is inclined to the foil[13].

(c) If a secondary reflection is excited in a nominally two-beam situation, the faint secondary images will be on opposite sides of the primary images of the components of the dipole[14].

None of these points is true of like pairs of dislocations. These criteria have been applied in the present work and the conclusions are that most dislocation pairs can be positively identified as dipoles, although in some cases what is observed is a double image of an undissociated dislocation. Figure 5.10 shows the change of spacing with sign of g and s. Figure 5.11 shows the centre of inversion in an oscillatory image. Figure 5.12 shows the secondary image effect at A. Figure 5.13 is indicative of dipole formation in the "curving back" behaviour of the dislocations. The separation of components, typically 500-1000Å also suggests dipoles. The expected equilibrium separation of like pairs should be much less, because the separation r decreases with order S, $r \alpha S^{-2}$ [15]. The absolute value of r depends on superlattice type but for s = 1 is likely to be <200Å.

There are pairs which look like dislocation of like sign. Figure 5.14 shows examples of images without a centre of inversion, and with small separations of the order of 80Å. Unambiguous identification is not possible. Certainly many more dipoles have been identified.

There remains the possibility of the components of the pairs themselves dissociating into half or quarter partials of much smaller separation, as discussed above.

In an attempt to resolve these partials the technique of weak-beam microscopy was used. Weak-beam microscopy has been used extensively in the last four years for the quantitative study of defect properties, and has recently been reviewed by Cockayne[17], who has done much of the theoretical analysis of the technique.

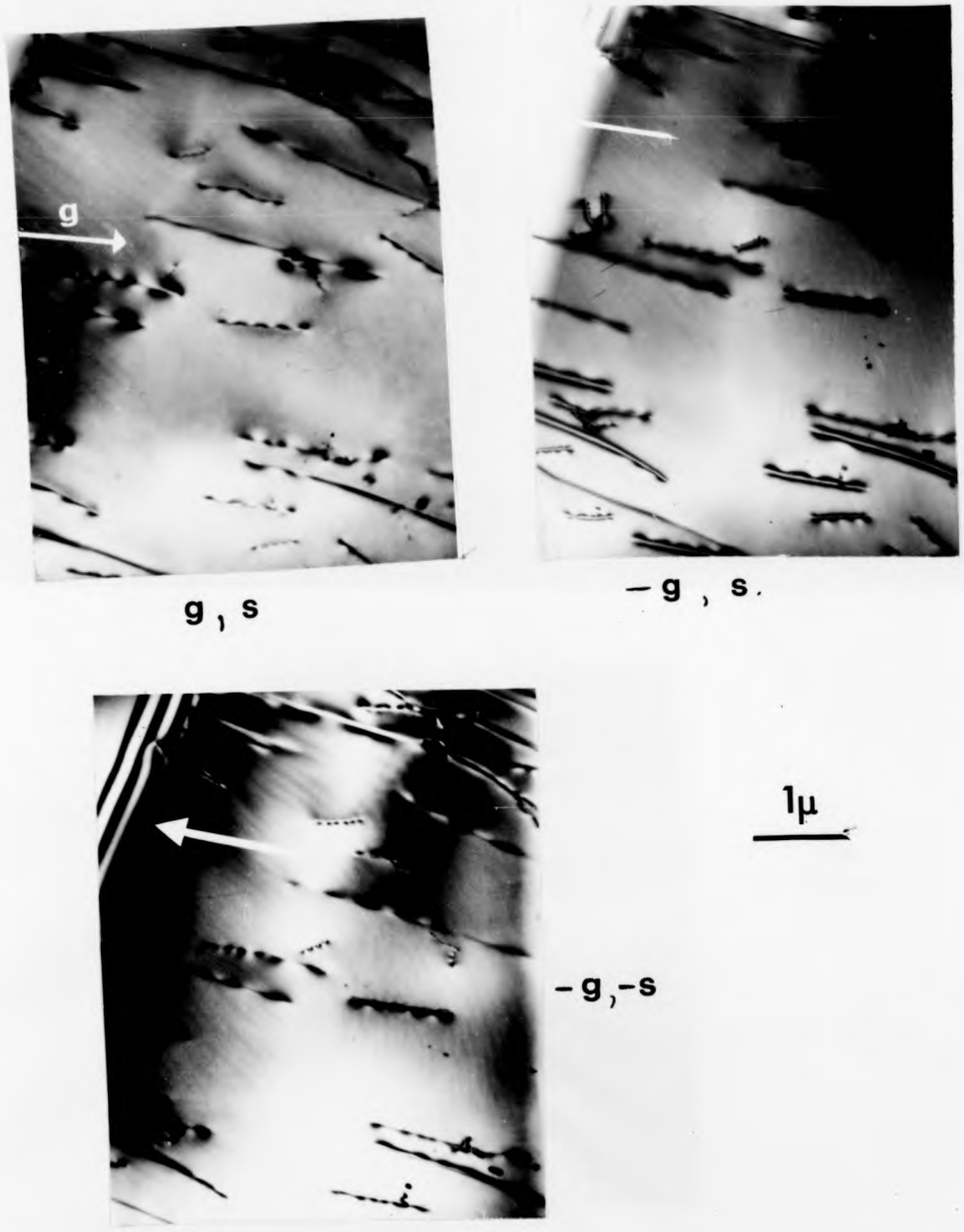

Fig. 5.10 Imaging of dislocation dipoles with changing sign of $\underline{g}$ and $\underline{s}$.

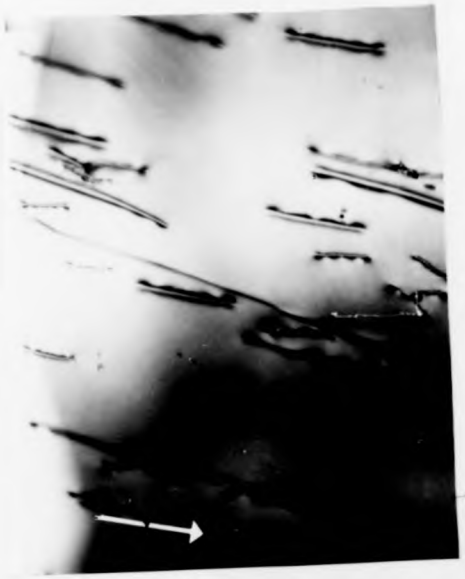

5.11

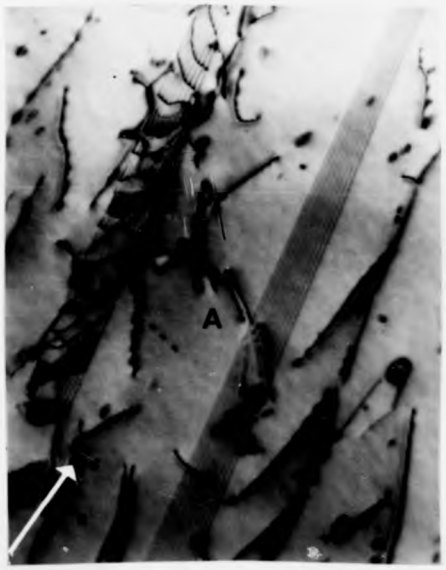

5.12

1μ

5.13

FIG. 5.11 Centre of inversion of image of inclined dipole.
FIG. 5.12 Secondary images of dislocation dipole at A.
FIG. 5.13 Formation of long loops.

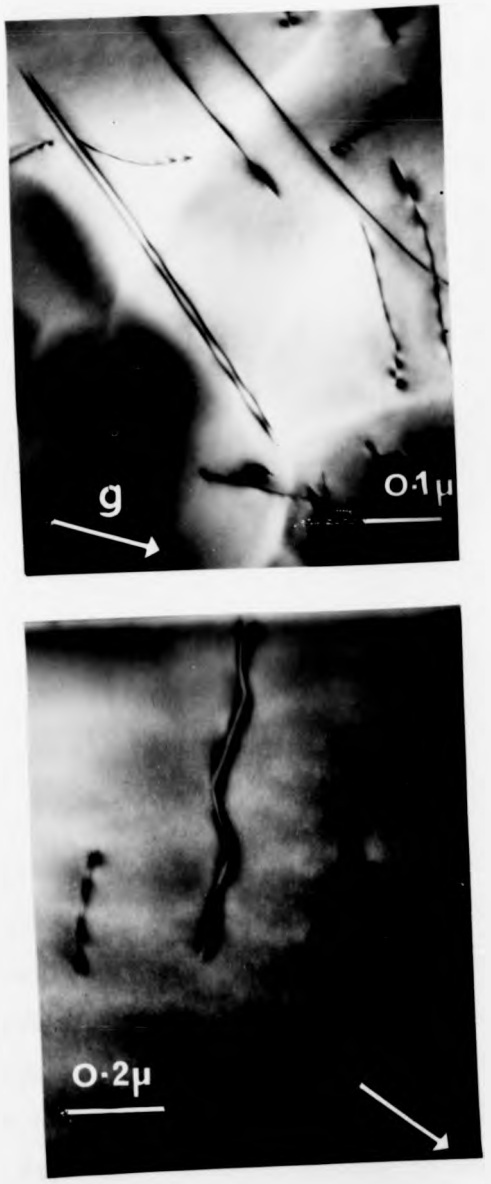

FIG. 5.14 Paired dislocations not exhibiting centre of inversion.

In weak-beam microscopy the deviation parameter S_g on the usual Ewald sphere model is set such that $/S_g/$ is large (greater than 2Å^{-1}) by exciting higher order reflections, and imaging in dark field using the first order reflection as in Fig. 5.15. Under these conditions large local strains are required to rotate the lattice into the Bragg condition and hence give a maximum diffracted intensity. Such strains occur for example, close to (<20Å from) a dislocation core, and it has also been shown[17] that the image will be sufficiently narrow to enable its position to be defined experimentally. This situation is ideal for the examination of defects where resolution of the order of 20Å is required, for example, resolution of partials in the present work. Weak-beam microscopy has been used[18] to confirm the four-fold dissociation into partials of superlattice dislocation in a range of iron-aluminium alloys with DO_3 type long-range order. Dissociations into partials have been predicted in other ordered alloys, for example Mg_3Cd[19], Ti_3Sn[20], but have not been directly observed, even by weak-beam methods.

Figures 5.16 and 5.17 show examples of weak-beam images in the present work. These show some suggestion of four-fold dissociation into partials of separation approximately 40Å but cannot be regarded as convincing evidence.

From Fig. 5.7 the possibility of the existence of enantiomorphic forms of VSi_2 can be deduced. The stacking sequence AB^1CAB^1CA has the same symmetry as VSi_2, the sense of the screw axis being reversed. The possibility of grown-in

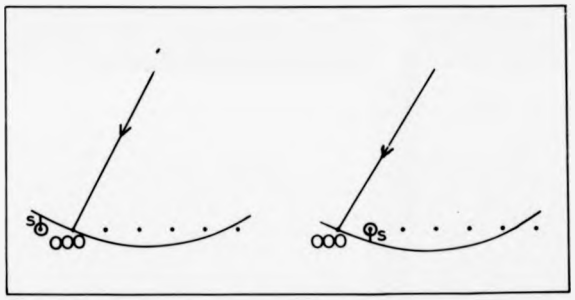

5.15

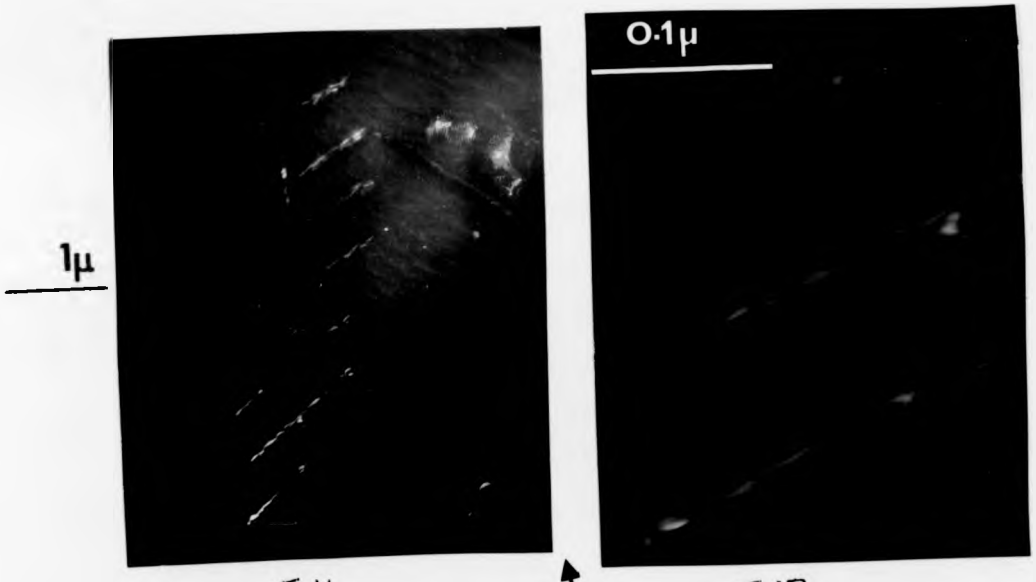

5.16 5.17

FIG. 5.15 Diffraction conditions for "weak-beam" imaging.

FIG. 5.16, FIG. 5.17 Weak-beam images in the present work.

interfaces between the two forms giving contrast in electron microscopy was investigated but not observed.

Sections were cut perpendicular to the basal plane to investigate the possible existence of non-basal dislocations with large Burgers vector as discussed in Chapter 6 below. In no case were such dislocations observed.

REFERENCES

(1) Wirkus, C. D. and Wilder, D. R. J. Amer. Cer. Soc. 49, 173 (1966).

(2) Kieffer, R. and Benesovsky, F. Iron and Steel Inst. Spec. Rpt. 58, 292 (1956).

(3) Berkowitz, J. B. Trans. Met. Soc. A.I.M.E. 233, 1093 (1965).

(4) Westbrook, J. H. and Wood, D. L. J. Nuc. Motor 12, 208 (1964).

(5) Schwettman, F. N., Groff, R. A. and Kolodney, M. J. Electrochem. Soc. 118, 1973 (1971).

(6) Nechiporenko, V. Izv. Ak. Nauk. SSR, Neorg. Mat. 3, 2283 (1967).

(7) De Vries, R. C. Trans. Brit. Cer. Soc. 53, 531 (1954).

(8) Whelan, M. J. In: "Modern Imaging and Diffraction Techniques in Materials Science". North-Holland (1970).

(9) Jones, P. J. and Edington, J. W. Phil. Mag. 25, 729 (1972).

(10) Head, A. K. Aust. J. Phys. 20, 557 (1967).

(11) Humble, P. Aust. J. Phys. 21, 325 (1968).

(12) Bell, W., Roser, W. R. and Thomas, G. Acta Met. 12, 1247 (1964).

(13) Forwood, C. T. and Humble, P. Aust. J. Phys. 23, 697 (1970).

(14) Fukamachi, M. Jap. J. App. Phys. 11, 1393 (1972).

(15) Stoloff, N. S. and Davies, R. G. Acta Met. 12, 473 (1964).

(16) Marcinkowski, M. J., Brown, N. and Fisher, R. M. Acta Met. 9, 129 (1961).

(17) Cockayne, D. J. H. J. Microscopy 98, 116 (1973).

(18) Crawford, R. C., Ray, I. L. F. and Cockayne, D. J. H. J. Microscopy 98, 196 (1973).

(19) Williams, J. C. and Blackburn, M. J. In: "Ordered Alloys". Claitors Pub. Dir. (1970).

(20) Jones, P. J. and Edington, J. W. Phil. Mag. 27, 393 (1973).

(21) Hayashi, Y., Delavignette, P. and Amelinckx, S. Phys. Stat. Sol. 42, 637 (1970).

APPENDIX

Calculation of Equilibrium Separation of Partial Dislocations

The equilibrium separation r of partials with Burgers vector b is given by

$$r = \frac{\mu b^2}{2\pi\gamma(1-\nu)} \qquad 5.5$$

where γ is the stacking fault energy, μ is the shear modulus and ν is Poisson's ratio for the material.

Assuming a relatively high value for stacking fault energy of 200 erg cm^{-2} since little stacking fault contrast is observed, a value of shear modulus of 10^{12} dyne cm^{-2} compared with 5×10^{11} for vanadium, and $\nu = 0.4$, then for half-partials, $b_{\frac{1}{2}} = 2.28$Å, $r \simeq 80$Å and for quarter-partials, $b_{\frac{1}{4}} = 1.25$Å, $r \simeq 20$Å.

CHAPTER 6

DISCUSSION OF EXPERIMENTAL OBSERVATIONS

In this chapter the results of Chapters 4 and 5 will be discussed in terms of crystal structure, bonding, defect structure and deformation mechanisms.

6.1 Deformation Geometry

The compression testing results show that slip on the basal plane in the direction of closest packing, i.e. the $\langle 11\bar{2}0 \rangle$ (0001) system, is the primary slip system operating in vanadium disilicide in the temperature range studied. The critical resolved shear stress τ_c on this system has been observed to be at least an order of magnitude less than on any other system. These observations can be explained in terms of the crystal structure of VSi_2. An analysis of dislocations in any crystal structure must consider dislocation stability and dislocation mobility.

6.1.1 Dislocation Stability

The strain energy of a dislocation can be considered as having two components - one due to small displacements outside the core, where elasticity theory can be applied, and the other due to the large displacements within the core. The former is usually much the larger contribution, in which case the strain energy is proportional to b^2 where $\underline{b}$ is the Burgers vector. However, in materials such as VSi_2 in which covalent bonding is significant, the core energy is sensitive to the direction of $\underline{b}$, and these variations in core energy because of the directed nature of the bonding can become very important.

In this case both contributions must be considered. In VSi_2 the shortest possible Burgers vectors and hence those having ...ely the lowest elastic displacement strain energy are the types $a/_3$ $\langle 11\bar{2}0 \rangle$ and C<0001>, i.e. a and c types, and also the (c + a) type which can be considered as the sum of the former two types. The Burgers vector for the a type is 4.571Å, and for c is 6.372Å. The elastic strain energy is therefore twice as great for c dislocations than for a dislocations. Even when dissociation of both types into partials is considered this factor is not much reduced. Unless the core energy of the $a/_3\langle 11\bar{2}0 \rangle$ dislocations is very much larger than that for c<0001> dislocations, the most stable dislocations will be of the a type.

The relative core structures of c and a dislocations may be assessed from the (0001) projection previously given (Fig. 5.7) and from a $\langle 10\bar{1}0 \rangle$ projection, Fig. 6.1. It can be seen that the a type contains fewer bonds than the c type dislocation. More atoms are therefore subjected to relatively large displacements by the motion of c-axis dislocations and the core energy is likely to be larger than for a-axis dislocations. The most stable dislocations in VSi_2 are therefore predicted from crystal structure considerations to be those of the type $a/_3\langle 11\bar{2}0 \rangle$, a-axis dislocations. This has been confirmed experimentally by transmission electron microscopy.

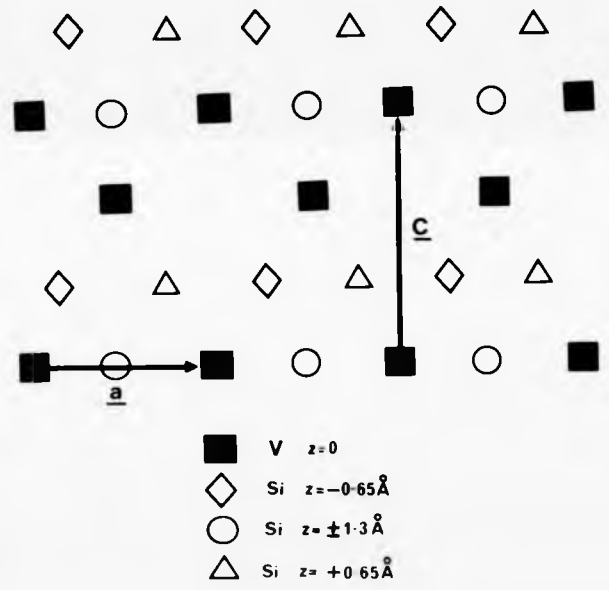

FIG. 6.1 $\{10\bar{1}0\}$ projection showing a and c dislocations

6.1.2 Dislocation Mobility

The simple Peierls model often gives a first approximation to the slip system containing the most mobile dislocations - the primary slip system. This model predicts that the stress τ_c to move dislocations is proportional to $\exp(-2\pi d/b)$ where d is the spacing between slip planes. Hence the most mobile dislocations are those with the smallest Burgers vector, i.e. for VSi_2 there will be a strong preference for slip on systems with a Burgers vector type, i.e. $^a/_3\langle 11\bar{2}0\rangle$ which has been shown above to be also the most stable Burgers vector. The primary slip plane will tend to be that with the largest inter-planar spacing. Unlike other more complex structures such as silicon nitride, Si_3N_4, this gives a meaningful prediction in VSi_2, in which being a "layer" structure, the basal-plane spacing is significantly larger than any other, e.g. from Figs. 5.7 and 6.1 the $\{10\bar{1}0\}$ planes have a separation of 0.65Å compared to 1.6Å for basal planes. From these considerations $^a/_3\langle 11\bar{2}0\rangle$ (0001) is predicted to be the primary slip system in VSi_2. This has been confirmed experimentally.

6.1.3 Non-basal Slip

Deformation results on specimens oriented for zero resolved shear stress on the basal plane suggested the possible operation of a secondary system at high stresses at temperatures above 1200°C. Electron microscopy on these specimens revealed basal dislocations only. Slip trace analysis on these specimens was extremely difficult because of the surface oxidation at these temperatures, although in one specimen (c-axis compression) slip-lines consistent with basal slip could just be detected.

There are three possibilities to explain the above observations in terms of the operation of the primary system only. ...ely

(a) Geometrical softening.

(b) Error in specimen orientation.

(c) Kinking - a localised geometrical softening.

(a) It has been shown (1) that in the case where the single active slip plane is aligned initially parallel to the compression axis so that the angle between the normal to the slip plane and the direction of compression equals 90°C, the shear stress acting on that system increases with deformation due to rotation of the crystal lattice, and plastic deformation can be initiated. This argument has recently been applied to the deformation of unfavourably oriented NiAl single crystals. (2) A recent paper by Reid[3] has shown that great care must be taken in applying the results of (1). He points out that (1) is valid for very small compressive strains only, and that in any practical case the resolved shear stress continuously diminishes as the crystal is compressed, regardless of orientation. What one can term "gross" geometrical softening is therefore ruled out as the explanation of the observed results.

(b) The effect of error in orientation of the specimen must be considered. Estimating the maximum error at about 2° from Laue photographs and subsequent orientation, cutting and polishing and re-photographing, the flow stress for basal slip, i.e. the total stress for c.r.s.s. on the basal system at 2° should be a factor of 35 higher than for crystals oriented for high c.r.s.s. on the primary system under otherwise identical conditions of strain rate and temperature. To

fit the experimental results reported here, an orientation error of about 6^{o} is required, which is much greater than any Lave observations made after specimen preparation. Slip because of orientation error was therefore discounted.

(c) Kinking is an extremely localised deformation occurring at inhomogeneities or stress concentrations in a crystal. It can occur simultaneously with uniform deformation, or on its own, in which case it can be considered as a form of geometrical softening in which a slip system is activated by an increasingly favourable orientation, but only locally.

In a compression test the end faces of the specimen are constrained so that they remain parallel to the faces of the anvils. To accommodate lattice rotation in the specimen, the ends of the specimen must be able to move laterally, i.e. there must be low friction between anvil and specimen. In the present work this is probably not the case, particularly at higher temperatures where there is some indication of reaction between anvil and specimen. This restraint of the specimen end-faces is not important at the low stresses employed for easy basal slip, but at higher stresses geometrical softening should be considered as a possibility. Gross geometrical softening has been ruled out but localised softening due to kinking at inhomonogeneities and subsequent operation of the primary basal slip system is very likely, and explains the present results. Additional experimental evidence in support of this is the macroscopic shape of some deformed crystals deformed in c-axis compression which indicates non-uniform deformation and kinking at one end of the specimen (Fig. 6.2).

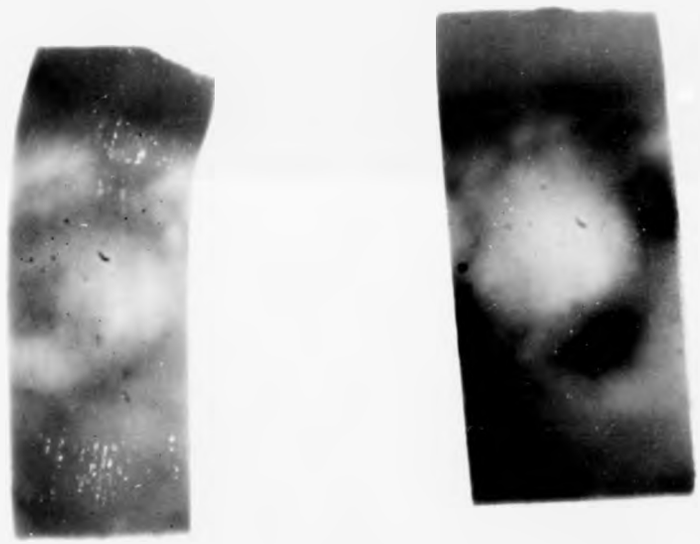

FIG. 6.2 Optical macrographs (x8) showing non-uniform deformation near the ends of compression specimens oriented for zero r.s.s. on the basal system.

It therefore seems probable that even in specimens oriented for near zero c.r.s.s. on the basal system, the basal primary slip system is the only one operating under the conditions of the present work.

6.2 Deformation Mechanisms

This section discusses the observed plasticity-initial flow and subsequent work-hardening - in terms of the motion and interaction of the basal dislocations of the single operating slip system.

6.2.1 Initial Flow

It should be noted that the values of flow-stress τ_c obtained in the present work are the stress values at which the stress-strain curve deviates from linearity for macroscopic deformation, i.e. when large numbers of dislocations are mobile. Thus the assumption implicit in much of the discussion of rate-controlling mechanisms that large numbers of dislocations are present is valid.

Because of the directional nature of the bonding in VSi_2, the mechanical properties of VSi_2 were expected to be markedly anisotropic, and this has been confirmed in the present work. In such a covalent crystal, the lattice friction stress is also expected to be high, and will be anisotropic. In these circumstances the most likely mechanism for initiation of plastic flow is the thermally activated overcoming of the energy barrier due to high lattice friction, i.e. a Peierls mechanism. This postulated mechanism may be tested by considering three sets of data obtained earlier.

(a) Effect of Temperature A high Peierls stress, together with a thermally activated overcoming of the Peierls barrier, implies a strong temperature dependence of the yield stress, even at high temperatures up to of the order of 0.5-0.6 T_m. This is in fact observed in Fig. 4.5.

The proposed Peierls mechanism is consistent with the observed brittleness of VSi_2 at temperatures below 700°C. This is due not to a discontinuity in the plastic deformation behaviour, but to the fact that at these temperatures the stress required to overcome the Peierls barrier to initiate plastic flow is so high that the competing mechanism of brittle fracture occurs.

The situation at temperatures higher than 0.5 T_m must be considered. At high temperatures the Peierls stress is very low, and there will be a temperature above which thermal fluctuations alone can overcome the Peierls barrier even in the absence of applied stress. In this situation, higher activation energy processes may become rate-determining. Consideration of this situation in carbides has been given by Harrod and Fleischer[4]. These workers estimate that the critical temperature for overcoming the Peierls barrier by thermal fluctuations alone lies in the temperature range 0.4-0.6 T_m, and they postulate that at higher temperatures diffusion processes such as climb become rate controlling. Diffusion data for silicides is not available, but a similar situation is possible.

Another possibility however, is that above the critical temperature for thermal overcoming of the Peierls barrier the athermal component of the stress, $\tau\mu$, given by

$$\tau_\mu = \tau - \tau^*$$

where τ and τ^* are the total stress and thermal component respectively becomes dominant. This is particularly relevant in the present work, as in the following section on work-hardening it will be shown that dipole interaction, an athermal process, is operational in VSi_2. At high temperatures therefore, dipole interaction may be the rate-determining deformation mechanism.

(b) Effect of Non-Stoichiometry The mechanical testing results of Chapter 4, as summarised in Fig. 4.6, show a marked reduction in τ_c for basal slip at any given temperature as the stoichiometric composition is approached from the silicon deficient side. This reduction in τ_c becomes less marked at higher temperatures.

As outlined in Chapter 1, the variation of strength with deviation from stoichiometry in intermetallic and interstitial compounds has received a certain amount of attention in the literature, and it has generally been found that such compounds increase in strength towards the stoichiometric composition. The two main classes of ceramics which have been investigated in this way are the refractory oxides, and the transition metal carbides.

The work of Nadeau[5] on oxygen-rich uranium dioxide UO_{2+x} is typical of the results obtained for oxides. He found a reduction in c.r.s.s. τ_c with increasing deviation from stoichiometry given by the relation

$$\tau_c \propto x^{-m}$$

where m at 1000°C had the value 0.13.

A Peierls mechanism was shown to be rate-controlling for plasticity of UO_{2+x} in this temperature range, and the softening effect of non-stoichiometry was attributed to enhanced double-kink formation due to non-stoichiometric defects with a consequent reduction in Peierls stress. Similar results are cited[5] for spinel, rutile, wustite and magnesia. Clearly, the present results on VSi_{2-x} do not permit this interpretation.

The work on non-stoichiometry in transition metal monocarbides[6-9] gives, in most cases, a softening of carbides with deviation from stoichiometry towards the carbon deficient side. An exception is the case of TaC_{1-x}[9] in which a strengthening towards off-stoichiometric compositions has been observed. This softening was initially attributed to enhanced diffusion rates. A series of papers by Lye and co-workers[10-12] has attempted to explain the whole question of the influence of non-stoichiometry on the strength of transition metal carbides in terms of crystal bonding and its effect on the Peierls stress. It is agreed that overcoming a Peierls barrier is the rate-controlling mechanism in plasticity of the carbides. An approximate band structure has been derived[10] for VC_{1-x}. The bonding in VC_{1-x} has been shown to arise primarily from interactions between orbitals on the V atoms. The strength of these bonds increases with carbon content because C atoms donate electrons and increase the number of 3d-electrons available for V-V bonding, and because the presence of carbon atoms in regions near V atom 3d-orbitals introduces a potential which increases the strength of V-V

interactions. This explains the increase of strength towards the stoichiometric composition. This effect should be applicable to transition metal carbides in general, although modified in detail by the characteristics of the different transition metal atoms. Although the general effect is one of softening with deviation from stoichiometry, the peak strength does not always occur at the stoichiometric composition, e.g. in VC_{1-x} the peak strength is found at $VC_{0.83}$. This has been explained by postulating that at this composition the 3d-electronic states, which have been shown to be most important in bonding in VC_{1-x}, are just filled. The anomalous behaviour of TaC_{1-x}[9] has been attributed[10] to differences in bonding caused by the band structure of Ta.

Since the overcoming of the Peierls barrier has been proposed as the rate controlling mechanism operating in the plastic deformation of vanadium disilicide in the temperature range studied, it must be shown that any increase or decrease of strength with composition is a consequence of a change in Peierls stress, i.e. the lattice friction stress which arises from electronic interaction between the constituent atoms in the lattice. Any change in Peierls stress must be explained, qualitatively at least in terms of inter-atomic bonding in the lattice.

Bonding in disilicides has been studied previously by calorimetric methods[13] as outlined earlier. This work showed that there is little or no metal-metal bonding in disilicides, the strong, directional, metal-silicon bond being dominant. The silicon-silicon bond lengths are considered to be determined largely by the strong metal-silicon bond. It is

the vanadium-silicon bond and the force required to break it which leads to the very high Peierls stress in vanadium disilicide and to the marked anisotropy in its mechanical properties.

The mode of accommodation of non-stoichiometry on the silicon-deficient side of VSi_2 could not be firmly established by the lattice parameter and density determination experiments described earlier (section 3.1.2). An increase of Peierls stress, i.e. an increase of density of vanadium silicon bonds could simply be achieved in a silicon-deficient situation by a V substitution for Si in the lattice, assuming the bonding character to be otherwise unchanged. In the case of accommodation by Si vacancies, established experimentally to be the more likely mechanism, the change in Peierls stress must be attributed to the V-□ bond being stronger than the V-Si bond. This is a reasonable deduction because the interatomic distances are expected to be smaller in the off-stoichiometric compositions with a consequent increase in bond strength. In the case of maximum deviation from stoichiometry, $VSi_{1.70}$, 15% of directional bonds are of the V-□ type.

(c) Activation Analysis The results of the activation analysis experiment reported in Chapter 4 may be used to make some deductions on the thermally activated deformation mechanism operating in VSi_{2-x}.

Several assumptions were made in deriving a value for the activation volume V^* at the onset of plasticity. It was assumed that the mobile dislocation density is stress independent, and that the stress is a unique function of strain rate and temperature. The activation analysis is by

definition an analysis of thermally activated mechanisms only, and throughout the work it has been assumed that the stress τ_μ required to overcome the athermal component of the force acting on the dislocations remains constant during differential strain rate tests. Finally, it is assumed that only one type of dislocation is important in the deformation process. Experimental evidence suggests that these assumptions are justified in the present work in the temperature range studied.

Table 6.1 shows the magnitude of activation volume V^* characteristic of various deformation mechanisms. The value of $20b^3$ for VSi_2 obtained in the present work should be compared to these characteristic values. The value obtained for V^* is consistent with point defect interaction, presumably Si vacancies. However, similar values of V^* were obtained for all compositions of VSi_{2-x} and in any case V substitution has been shown to be the most probable mechanism for accommodation of non-stoichiometry. Dislocation intersection is certainly not important here as no non-basal dislocations have been observed. Climb is unlikely to be rate-controlling at these temperatures, and cross-slip in VSi_{2-x} is likely to be very restricted because of the high c.r.s.s. on secondary systems. The values of V^* for jog motion and dipole intersection are very much larger than that obtained here. The activation results support the proposal of a Peierls mechanism being rate-controlling at the onset of plasticity. The low value obtained for V^* indicates a strong strain-rate dependence of the yield stress τ_c similar to that observed in covalent

Mechanism	V (b^3)	Comments
Peierls	1-20	V^* independent of strain
Point defect drag	10^3	Usually edge dislocation
Point defect interaction	1-10	V^* α defect concentration
Dislocation intersection	10^3	V^* depends on strain
Climb	1	Edge dislocations only
Jog motion	10^3	Screw dislocations only
Cross-slip	10^2	Often rate-controlling when dislocations are extended
Intersect dislocation dipoles	$>10^3$	V^* decreases as dipole density increases with strain

TABLE 6.1 Characteristic values of activation volume of various mechanisms

crystals such as Ge, and is characteristic of a Peierls mechanism.

6.2.2 Work-Hardening

The experimental observations show the characteristic form of the stress-strain curve for VSi_2 (Fig. 4.4) to be an elastic region with a single yield point followed by a two-stage work-hardening curve - Stage I of relatively high work hardening rate typically up to 10% shear strain followed by Stage II, almost zero work-hardening, at higher strains.

The main mechanisms of work hardening are dislocation interaction and dislocation intersection to form sessile configurations. Work-hardening can be enhanced by point defect or precipitate interaction with slip dislocations, but these processes cannot directly give rise to work-hardening.

In VSi_2, in which a single slip system only has been shown to operate in the temperature range studied, the intersection of glide dislocations can only be with grown-in non-basal dislocations which have been observed only in extremely low density. This type of mechanism can therefore be neglected.

In view of the evidence presented in Chapter 5 of the formation of dislocation dipoles, a model for the work-hardening behaviour of VSi_{2-x} which suggests dipole formation as the operative mechanism is proposed.

Firstly, the mechanism of the formation of the observed dislocation dipoles in VSi_{2-x} should be considered. A simple edge-trapping mechanism is likely to be the initial step, A model for the development of the observed dipole structures

is shown in Fig. 6.3, (a) the edge components of the slip dislocations on the basal plane trap each other. Simultaneously the screw portions also trap each other but are annihilated by climb (b) at higher stresses segments of large separation form long segments of smaller separation by climb (c) at even higher stresses break-up of these segments into loops occurs, followed by annealing out of the loops. This model is consistent with the experimental observations in Chapter 5. Each of the above stages has been observed. Figure 5.6 shows the trails of loops characteristic of specimens strained to high levels. Long segments of narrow separation are frequently observed (Fig. 5.12).

Many of the dipoles observed are not unambiguously pure edge dipoles showing that annihilation of the screw components of mixed dislocation dipoles has not been completed. The following discussion of the effect of dipole formation on mechanical properties will be given in terms of edge components alone, on the assumption that since screw components have no stable equilibrium position, annihilation or repulsion will eventually occur with little effect on deformation.

The effect of dipole formation on plasticity and work-hardening is suggested to be as follows:- plasticity is initiated when the applied stress is equal to the lattice frictional (Peierls) stress. For small plastic strains the average vertical separation of dislocations, i.e. in this case the separation of parallel slip planes containing dislocations is large, of the order of 2000Å. With increasing plastic strain this vertical separation decreases to of the order of 500Å. Figure 6.4 shows the effect of this decrease in vertical separation on dipole formation. The force per unit length F_m between two parallel edge dislocations is given by

$$F_m = \frac{\mu b^2}{2\pi(1-V)r} \cos\theta(\cos^2\theta - \sin^2\theta) \quad 6.1$$

where μ is the rigidity modulus and V is Poisson's ratio. Figure 6.4 illustrates this situation for edges of opposite sign for which there are positions of stable equilibrium at

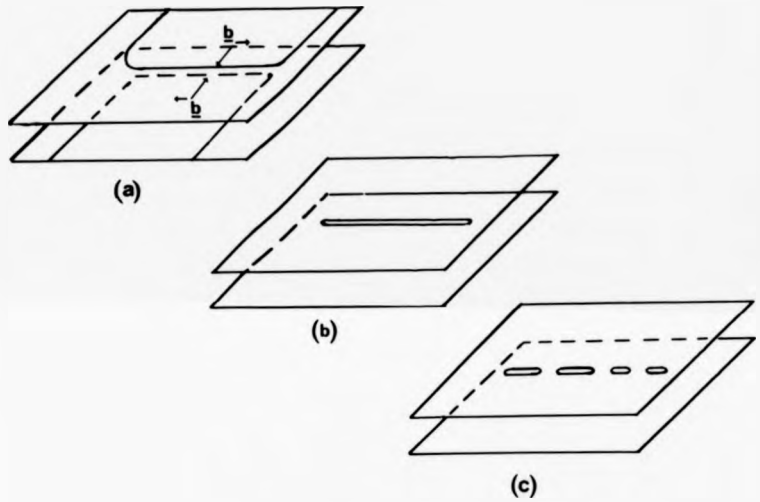

FIG. 6.3 Edge-trapping model for dipole formation.

(a) Trapping of dislocations

(b) Formation by climb of long dipole segments

(c) Break-up by climb of dipoles into loops.

$\theta = \frac{\pi}{4}$ and $\frac{3\pi}{4}$. Figure 6.4 shows the force between edges in equilibrium on slip planes a distance y_o apart. The force is given in units of $\mu b^2/2\pi(1-\nu)y$. For a yield stress $\tau\mu$ of $10^{-3}\mu$, edge dipoles are therefore likely to be stable if the components lie on slip planes which are less than 800-1000Å apart, i.e. dipole stability and hence work-hardening increases with increasing stress. Dipoles are obstacles to glide dislocations. As deformation proceeds dipole density increases, and dipole separation decreases, both leading to an increase in the resistance to dislocation motion. This results in the observed stage I (high) work-hardening.

With increasing stress, recovery becomes important. Edge dipoles are stable only when their width d satisfies the relation $d < (\mu/b)/8\pi(1-\nu)(\tau - \tau_c)$ 6.2

As the applied stress τ increases, the maximum stable dipole width decreases and wider dipoles break up by glide. The importance of climb in dipole formation in the present work has been emphasised above. At high stress, narrower dipoles may break up by climb into loops to reduce their line energy. Both these processes lead to a reduction in dipole density, and a dynamic work-hardening-recovery process occurs involving the formation of edge dipoles by edge trapping of slip dislocations, and their break-up by climb or glide, giving the observed Stage II (virtually zero) work-hardening.

The lack of slip flexibility in VSi_{2-x}, i.e. the operation of a single slip system only in the temperature range studied has important consequences for both dipole formation and break-up. Because of the high yield stress

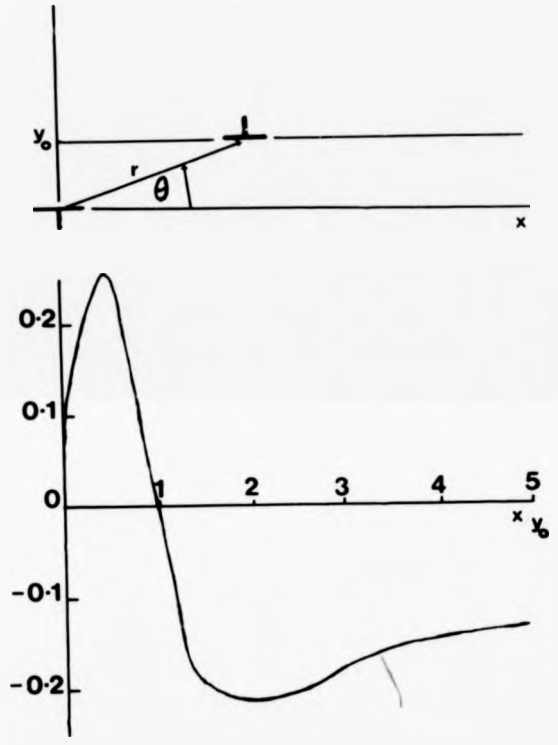

FIG. 6.4 Force between parallel edge dislocations on slip planes a distance y_o apart.

Force in units of $\mu b^2/2\pi (1-\nu)y$

τ_c on secondary slip planes cross-slip is likely to be inhibited. This is very different from h.c.p. metals in which recovery by cross slip is important in basal deformation. In the present work dipole formation and subsequent break-up into loops is much more likely to be achieved by dislocation climb. Another consequence of the high τ_c for secondary systems is that dissociation of dipoles by glide at high stress levels must be inhibited by the sessile nature of the dipole segments not lying within the primary (0001) plane. A similar phenomenon has been observed in basal glide in Mg[14]. In the present model therefore recovery must be achieved mainly by a climb process. The effect of temperature and composition on the work-hardening curves lends support to recovery by climb. For a given composition, with increasing temperature Stage II hardening occurs at lower strains (Fig.4.8) suggesting a strong temperature dependence of the recovery process, which points to climb rather than glide cross-slip as the relevant mechanism. The effect of composition is not so clear-cut, but the tendency is for Stage II hardening to commence at slightly lower strains with increasing deviation from stoichiometry (Fig. 4.9). This effect might be due to enhancement of diffusion in VSi_{2-x} with increasing X.

The above model fits the experimental results on vanadium disilicide closely. The problem of high work-hardening rate occurring in a crystal with a single slip system only operating has been considered by Marcinkowski and co-workers[15,16], They have given[15,16] a general theoretical treatment of the influence of dipoles and larger arrays of dislocations

in ordered alloys. The present model may be considered as a special case of this general treatment in that similar concepts such as dipole widths and their variation with stress have been applied. A similar model has also recently been applied[17] to sapphire (Al_2O_3) deformed at 1200° to 1500°C by basal slip. This work considers dipole formation and based on the work of Tetelman[18] proposes an edge-trapping mechanism involving cross-slip. Clearly this type of work-hardening model is applicable mainly to highly anisotropic materials, i.e. ceramics. In h.c.p. metals such as Mg[14], Zr[18], and Be[19] the existence of secondary slip systems whose τ_c is more comparable with that for the primary system than in VSi_{2-x} means that intersections of dislocations to form sessile configurations and cross-slip are very important.

The low dislocation densities observed in the electron microscope studies (Chapter 5) have not been explained in this model. It is perhaps surprising that a process involving high work-hardening and dynamic recovery should be possible at such low dislocation densities as have been the case. The explanation probably is either that many dislocations anneal out after formation of loops from dipoles by climb or that the large strain field for large $\underline{b}$ gives large dipole separations.

REFERENCES

(1) Bowen, D. K. and Christian, J. W. Phil. Mag. 12, 369 (1965).

in ordered alloys. The present model may be considered as a special case of this general treatment in that similar concepts such as dipole widths and their variation with stress have been applied. A similar model has also recently been applied[17] to sapphire (Al_2O_3) deformed at 1200° to 1500°C by basal slip. This work considers dipole formation and based on the work of Tetelman[18] proposes an edge-trapping mechanism involving cross-slip. Clearly this type of work-hardening model is applicable mainly to highly anisotropic materials, i.e. ceramics. In h.c.p. metals such as Mg[14], Zr[18], and Be[19] the existence of secondary slip systems whose τ_c is more comparable with that for the primary system than in VSi_{2-x} means that intersections of dislocations to form sessile configurations and cross-slip are very important.

The low dislocation densities observed in the electron microscope studies (Chapter 5) have not been explained in this model. It is perhaps surprising that a process involving high work-hardening and dynamic recovery should be possible at such low dislocation densities as have been the case. The explanation probably is either that many dislocations anneal out after formation of loops from dipoles by climb or that the large strain field for large $\underline{b}$ gives large dipole separations.

REFERENCES

(1) Bowen, D. K. and Christian, J. W. Phil. Mag. 12, 369 (1965).

(2) Fraser, H. L., Loretto, M. H. and Smallman, R. E. Phil. Mag. 28, 667 (1963).

(3) Reid, C. N. Phil. Mag. 27, 499 (1973).

(4) Harrod, D. L. and Fleischer, L. R. In: Anisotropy in Single Crystal Refractory Compounds, Plenum Press, N.Y., Vol. I, 341 (1969).

(5) Nadeau, J. S. J. Amer. Cer. Soc. 52, 1 (1969).

(6) Williams, W. S. J. App. Phys. 35, 1329 (1964).

(7) Lye, R. G. and Logothetis, E. M. Phys. Rev. 147, 622 (1966).

(8) Hollox, G. E. and Smallman, R. E. Proc. Brit. Cer. Soc. 6, 317 (1966).

(9) Steinitz, R. In: Proc. Conf. on Nuclear Applications of Non-fissionable Ceramics, Washington; A.N.S. Illinois (1966).

(10) Lye, R. G., Hollox, G. E. and Venables, J. D. In: Anisotropy in Single Crystal Refractory Compounds, Plenum Press, N.Y., Vol. I, 445 (1969).

(11) Lye, R. G. In: Atomic and Electronic Structure of Metals, A.S.M., Cleveland (1967).

(12) Rowcliffe, D. J. and Hollox, G. E. J. Mat. Sci. 6, 1270 (1971).

(13) Robins, D. A. and Jenkins, I. Acta Met. 3, 598 (1955).

(14) Sharp, J. V. and Christian, J. W. Phys. Stat. Sol. 11, 831 (1965).

(15) Marcinkowski, M. J. and Lasko, G. J. App. Phys. 38, 2129 (1967).

(16) Sadananda, K. and Marcinkowski, M. J. J. App. Phys. 44, 1989 (1973).

(17) Pletka, B. J., Mitchell, T. E. and Heuer, A. H. J. Amer. Cer. Soc. 57, 388 (1974).

(18) Akhtar, A. Acta Met. 21, 1 (1973).

(19) Conrad, H., London, G. and Damiano, V. In: Anisotropy in Single Crystal Refractory Compounds, Plenum Press, N.Y., Vol. 1, 153 (1969).

CHAPTER 7

SUMMARY AND CONCLUSIONS

7.1 Summary of Results on VSi_{2-x}

I. Large, high-purity single crystals of vanadium disilicide have been grown, with various compositions within the range of single-phase stability, by Czochralski pulling from a melt contained in a water-cooled copper hearth.

II. The homogeneity range of VSi_{2-x} has been determined by X-ray methods to be $VSi_{1.70}$ to $VSi_{1.95}$ and silicon vacancies has been postulated as the mechanism of accommodation of non-stoichiometry

III. A programme of single crystal compression testing has been carried out on crystals of selected compositions across the homogeneity range in the temperature range 600°C to 1200°C. The results of this programme showed that basal slip is the primary slip system operating in VSi_{2-x}, and that the critical resolved shear stress τ_c for possible secondary systems is at least an order of magnitude greater than for basal slip at the same temperature up to 1200°C. Data has been presented on the variation of c.r.s.s. for basal slip with composition and temperature.

IV. Transmission electron microscopy has been used to confirm the experimental data on deformation geometry. In addition electron microscopy contrast studies have yielded evidence on the dislocation structure in vanadium disilicide.

V. A model has been proposed for the plasticity of VSi_{2-x}. Plastic flow is initiated by thermal overcoming of a Peierls

barrier, and the subsequent two stage work-hardening behaviour has been explained in terms of dislocation dipole formation followed by a dynamic recovery process involving dipole break-up by climb.

7.2 Disilicides as Engineering Materials

The broad aim of the work presented in this thesis is to evaluate transition metal disilicides as high-temperature engineering materials.

The following sections use the results of the present work on vanadium disilicide as a model disilicide to carry out this assessment.

7.2.1 VSi_{2-x} as a Model Disilicide

As described in detail in Chapter 1, the disilicdes of transition metals all have closely related crystal structures consisting of stacking sequences of similar close-packed Me-Si layers. The stacking sequences vary only in the number of layers forming each sequence. Two- three- and four-fold repeat stacking sequences are found. The question here is the validity of extrapolating the present results on VSi_2 to transition metal disilicides generally. Since the results as discussed fully in Chapter 6 showed that plasticity occurs by deformation in the basal plane alone, it is apparent that all disilicides should behave very similarly to VSi_{2-x} since the basal planes are in each case virtually identical, and bonding between basal planes will be similar in each case. The main features of the proposed model for the plasticity of VSi_{2-x} - Peierls barrier, dislocation dipole trapping and

barrier, and the subsequent two stage work-hardening behaviour has been explained in terms of dislocation dipole formation followed by a dynamic recovery process involving dipole break-up by climb.

7.2 Disilicides as Engineering Materials

The broad aim of the work presented in this thesis is to evaluate transition metal disilicides as high-temperature engineering materials.

The following sections use the results of the present work on vanadium disilicide as a model disilicide to carry out this assessment.

7.2.1 VSi_{2-x} as a Model Disilicide

As described in detail in Chapter 1, the disilicdes of transition metals all have closely related crystal structures consisting of stacking sequences of similar close-packed Me-Si layers. The stacking sequences vary only in the number of layers forming each sequence. Two- three- and four-fold repeat stacking sequences are found. The question here is the validity of extrapolating the present results on VSi_2 to transition metal disilicides generally. Since the results as discussed fully in Chapter 6 showed that plasticity occurs by deformation in the basal plane alone, it is apparent that all disilicides should behave very similarly to VSi_{2-x} since the basal planes are in each case virtually identical, and bonding between basal planes will be similar in each case. The main features of the proposed model for the plasticity of VSi_{2-x} - Peierls barrier, dislocation dipole trapping and

subsequent recovery by climb are therefore equally applicable to all the layer type transition metal disilicides, and any predictions based on results on vanadium will be valid for other cases.

7.2.2 Single Crystal Material

The single crystal deformation results show that, as predicted from the crystal structure, disilicides have very good oxidation resistance and chemical stability, and anisotropic mechanical properties.

In orientations with zero resolved shear stress on the basal plane VSi_2 shows no plasticity up to 1200°C, and can therefore be regarded as a brittle material with extremely good oxidation resistance. Failure is likely to be by brittle fracture at high stress levels although stress relief by localised plastic flow is possible.

In other orientations VSi_2 exhibits plasticity at temperatures above 700°C at moderately high c.r.s.s., and retains this strength to higher temperatures.

Single crystal disilicides are therefore potentially useful high-temperature materials, but only for small, specialised components where oxidation/chemical resistance with high strength but perhaps some ductility at high stresses is required. The difficulty, and hence expense, of single crystal components precludes more general applications.

7.2.3 Polycrystalline Material

Single crystal deformation geometry is used to predict the behaviour under stress of polycrystalline disilicides. In a polycrystalline disilicde the grains will be randomly or

near randomly oriented, and hence at high temperatures and stresses will undergo plastic flow by basal slip. For a polycrystal to be capable of large plastic changes of shape by glide within the grains without failure by formation of internal cavities, the von Mises criterion of five independent slip systems operating must be satisfied. The observation that in the temperature range studied basal slip only, i.e. two independent slip systems, is operative, implies that polycrystalline vanadium disilicide is incapable of plastic deformation by glide, and is therefore predicted to fail by the formation of internal cavities and to have only limited ductility prior to failure.

The above discussion refers to deformation by glide alone. Groves and Kelly[1] have pointed out that at high temperatures the possibility of dislocation climb enabling general shape changes to take place in crystals with fewer than five independent slip systems should be considered. They show that ceramic materials such as sapphire, graphite and β quartz, which have fewer than the requisite five operative slip systems area at high temperatures, do in fact exhibit macroscopic slip at temperatures about 0.5 T_m . For fine-grained (<50 μm) materials these results may be explained in terms of Nabarro-Herring vacancy creep[2] in which strain is produced by diffusion currents at grain boundaries. This mechanism cannot explain the macroscopic deformation observed in coarse-grained materials. Dislocation climb had been suggested[3] as the rate-controlling mechanism in this case. Groves and Kelly[1] show that dislocation climb can in fact produce strain-rates of the order of magnitude observed, and also that

dislocation climb can produce macroscopic strain. They show that dislocation climb can produce a general strain given six Burgers vectors, no four of which are co-planar. This is clearly a rigorous requirement unlikely to be found in ceramic materials with limited slip flexibility. A more relevant case is the possibility of a combination of glide and climb producing a general strain. This has been shown[1] to be possible if the crystal possesses three non-co-planar Burgers vectors, and this mechanism has successfully been applied to the cases quoted above.

Applying the above considerations to the case of vanadium disilicide, it has been shown earlier (section 6.2.2) that dislocation climb may well be important in VSi_2 even at temperatures below 0.5 T_m . However, electron microscopy has not revealed dislocations with the four different Burgers vectors required in addition to basal slip for a general shape change. Macroscopic slip in coarse-grained VSi_2 seems unlikely even when climb is considered, although it may be possible at higher temperatures. In fine-grained disilicides however, deformation by diffusional creep, particularly at high temperatures, is probable.

Single-phase, fine-grained disilicides are therefore potential high-temperature engineering materials, and should show appreciable ductility at temperatures >0.5 T_m .

7.2.4 Composites Containing Disilicides

As pointed out in Chapter 1, strengths near the theoretical have been achieved in ceramic materials in the form of single crystal fibres, free of surface imperfections. A promising

way of utilising inherently strong solids of limited slip flexibility such as VSi_2 would be in the form of single crystal whiskers or fibres, aligned, parallel to the direction of application of the load, in a suitable matrix.

The theory of fibre reinforcement of a matrix is well established and has recently been reviewed[4]. A parallel bundle of brittle fibres is much less sensitive to cracking than bulk material, since the geometry ensures that a crack will be very short, across a single fibre only, or parallel to a fibre axis and hence harmless.

A suitable matrix is necessary to bind the fibres together For high temperature materials, a metallic matrix is an obvious choice, and is in any case a suitable choice, since a ductile matrix can relieve stress concentrations at the tips of fibres under load by plastic flow.

Reinforcement of metals by aligned fibres is therefore a promising route to high temperature materials.

There are two distinct ways of producing such composite materials - the alignment of pre-fabricated fibres in a metallic matrix, and <u>in situ</u> growth by undirectional solidification of a eutectic of suitable composition and morphology.

The former technique has been used for fibres of C, B, Si and Al_2O_3, but for intermetallics and interstitials the difficulty of fabricating fibres precludes the use of this method.

Undirectional solidification of eutectics has been extensively studied[5] and it has been shown that under the correct conditions a regular fibrous morphology may be obtained. This technique has the advantage that a strong

fibre-matrix interface is guaranteed, as is stability at high temperatures, and the disadvantages that very careful preparation is required, and that the volume fraction and crystallographic orientation of the phases is fixed.

Eutectic solidification with vanadium disilicide as the minor, fibrous phase is a very possible high-temperature material-production technique. The theory of eutectic solidification shows that the required regular fibrous morphology can be obtained only if the volume fraction of the minor phase is $\leq$ 28%, otherwise an irregular morphology or a regular lamellar morphology is produced, both of which are much less desirable from the mechanical properties point of view.

If a suitable eutectic containing a disilicide as the minor phase can be unidirectionally solidified, it is highly probable that the fibre axis, i.e. the growth axis, would have a preferred orientation close to the c-axis, as in the crystal growth described in this thesis. This situation would be ideal, as from the single crystal deformation work fibres loaded parallel to the c-axis would be very strong indeed since there is zero resolved shear stress on the basal system. A composite consisting of a metallic matrix containing single crystal disilicide fibres oriented close to the c-axis is a most attractive high-temperature material.

The oxidation resistance and thermal shock of the disilicide have been shown to be good as is the high temperature strength in this orientation. The metallic matrix has also reasonably good high temperature properties, can accommodate

stress concentrations by plastic flow and does not lower significantly the strength to weight ratio of the composite.

The achievement of this disilicide composite cannot be by solidification of a binary eutectic, as the disilicide occurs at the silicon-rich end of the phase diagram. In some binary transition metal-silicon systems there is a suitable eutectic between the parent metal and the intermediate silicide, e.g. in the titanium-silicon system the eutectic Ti-Ti_5Si_3 exists, and has been shown to have regular fibrous morphology when solidified under suitable conditions[6,7], with the fibre axis close to a c-axis orientation.

In the case of disilicides, solidification of a suitable ternary eutectic is the obvious route, with another transition metal as the third component to optimise the properties. Nickel would be a sensible choice as in Mo-Ni-Si[8].

Summarising, the use of disilicides as structural materials seems to be confined to components made by careful solidification of either single crystal or eutectic composites, both of which have excellent high temperature properties or to fine-grained polycrystals where greater plasticity can be tolerated. The need for careful preparation precludes the application of disilicides on a large scale, and small components for highly specialised applications seem to be the main area for use of disilicides as structural materials.

7.3 Possible Future Work

I. Solidification of selected ternary eutectics.

II. Mechanical testing of suitable composites.

III. Investigation of possible interesting electrical properties of fibrous composites containing disilicide fibres.

IV. Study of behaviour of fine-grained polycrystalline disilicides.

REFERENCES

(1) Groves, G. W. and Kelly, A. Phil. Mag. 19, 277 (1969).

(2) Herring, C. J. Appl. Phys. 21, 437 (1958).

(3) Warshow, S. I. and Norton, F. H. J. Amer. Cer. Soc. 45, 479 (1962).

(4) Kelly, A. Met. Trans. 3, 2313 (1972).

(5) Hogan, L.M.,Kraft, R. W. and Lemkey, F. D. Adv. Mat. Res. 5, (1971).

(6) Crossman, F. W. and Yue, A. S. Met. Trans. 2, 1545.(1971).

(7) Prud'homme, M., Lavelle, B., Pieraggi, B. and Dabosi, F. J. Crystal Growth 18, 273 (1973).

(8) Savitskii, E. M. Russ. J. Inorg. Chem. 7, 573 (1962).